POLITEHNICA **National University of Science and Technology from Bucharest**

Faculty of Industrial Engineering and Robotics

Department of Strength of Materials

Ph. D. THESIS

Research on some structural elements dedicated to impact energy absorption to railway vehicles

(summarized)

Author:

Physics Eng. Dan-Mihail COSTESCU

Scientific tutor:

Prof. Dr. Eng. Anton HADĂR

Bucharest – 2023

Keywords: *collision, railway vehicles, impact energy, controlled plastic deformation*

Content

Page

Chapter 1

General considerations

1.1 Trends in the development of impact energy absorbing elements in railway vehicles

1.1.1. The current stage of the production of impact energy absorbing elements for railway vehicles

The rail industry is growing globally, achieving economic development and environmental benefits by providing safe and sustainable networks. Traffic volumes and rail transport speeds, for both passenger and freight trains, are increasing and require superior protection for passengers as well as to meet operability and maintainability standards with low life cycle costs.

Crash technology is a method of controlled transfer and absorption of very high impact energy under highspeed collision conditions. It was developed to increase the level of passive safety in rail transport.

The European standard EN 15227:2020 defines the crash safety requirements for railway vehicles bodies. The standard applies to locomotives, passenger trains, underground trains and trams.

According to the latest railway regulations, wagons carrying dangerous goods already in use must be able to absorb at least 500 kJ per wagon end and new wagons must be able to absorb at least 800 kJ per wagon end. The purpose of imposing these requirements is to ensure adequate accidental impact protection for speeds above 12 km/h. To comply with these regulations, existing wagons must be equipped with impact buffers of at least 250 kJ, while new wagons have impact buffers of at least 400 kJ.

Worldwide, in the last decade, a number of railway manufacturers, with a lot of experience in the field, began to be actively involved in finding reliable technical solutions, as simple and cheap as possible, to manufacture impact energy absorbing elements to railway vehicles. They collaborated with research and development units and higher education institutions and provided the material basis and funds necessary for the successful implementation of this activity.

A. *SC INNOVA Systems and Technologies SRL from Arad, Romania*

The company was established in 2005 under the leadership of the founder, mechanical engineer Dimitrie Otlăcan, who has a vast experience, over four decades, in the design of freight and passenger wagons. Since its founding, one of the main concerns has been the creation of a national crash buffer. For this, countless tests have been done over the years, with various prototypes, finally resulting in a series of products at the highest levels of international standards.

Most wagons in the operators' fleets in Romania are currently equipped with standard category A buffers of 30 kJ. The 150 kJ buffer (fig. 1), developed and manufactured by INNOVA, has a dynamic capacity five times that of a

standard category A buffer and twice that of a category C buffer. Real impact tests recorded over 200 kJ of absorbed energy on the buffer.

Fig. 1 *- INNOVA buffer of 150 kJ*

The 400 kJ buffer, developed and manufactured by INNOVA, can absorb over 400 kJ per buffer, which means over 800 kJ per car end. Official tests recorded 478 kJ on the buffer.

The INNOVA 400 kJ buffer (fig. 2) is suitable for fitting both existing and new wagons. The product fully complies with all the conditions imposed by the European profile standards in force.

Fig. 2 *- The 400 kJ INNOVA buffer*

INNOVA 150 kJ and 400 kJ buffers are equipped with thermoplastic/polymer shock absorbers (manufactured by MINER TecsPak , Durel DP 30).

The deformation of the buffer includes two stages:

- elastic deformation, observed at impact speeds below 12 km/h and at forces not exceeding 1.5 MN;
- elastic + plastic deformation, generated at impact speeds exceeding 12 km/h and forces over 1.5 MN (fig. 3 and fig. 4).

The buffers are made of a welded assembly, having a 450 mm long, removable plate of S355J2 steel. The following additional options are available upon request:

- an additional manganese steel wear plate;
- an extra long buffer plate of 550 mm.

***Fig. 3** - INNOVA buffer of 150 kJ after deformation*

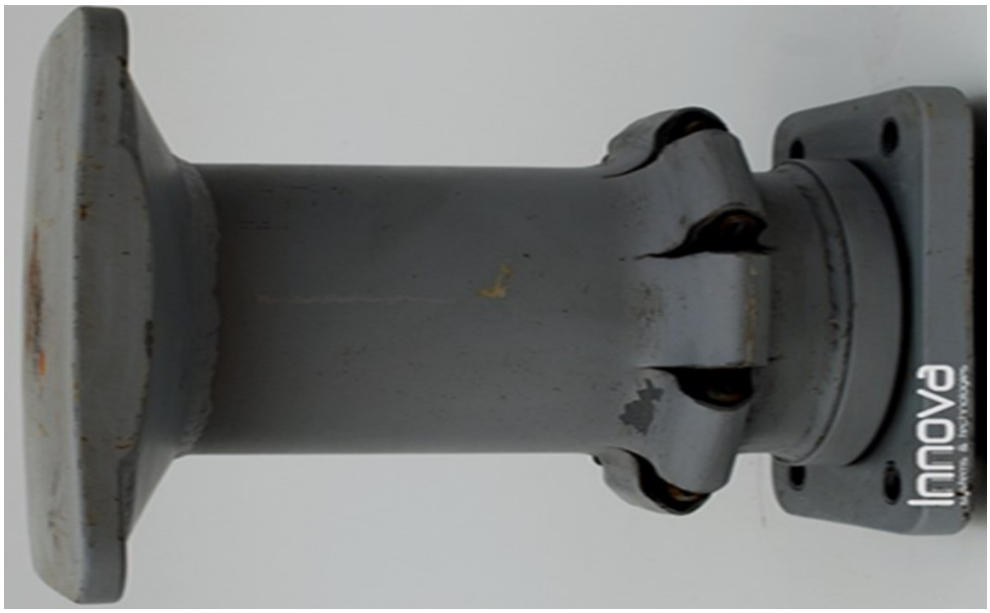

***Fig. 4** - INNOVA buffer of 400 kJ after deformation*

B. *EST Eisenbahn-Systemtechnik GmbH , Germany*

The company EST Eisenbahn-Systemtechnik GmbH was founded in 2001 in the small German town of Wangen im Allgäu .

Crash buffer manufactured by EST combines, in a single component, a standard railway vehicle buffer and an energy-absorbing deformation element. It is characteristic that the additional function, as a deformation element, is integrated into the buffer housing, so that no additional space is needed after deformation. The external dimensions and attachment flange of the EST crash buffer are identical to those of a classic buffer, which complies with the railway industry standard UIC 526-1.

The EST crash buffer can be fitted to all vehicles that have been designed for classic buffers in accordance with this standard. This buffer can be used for the protection of modern railway vehicles with high capital costs as well as older rolling stock where increased protection is desired.

The crash element function of the EST crash buffer prevents overloading of the vehicle, its structure and its components during heavy impacts and collision events. Thus, peak loads and high accelerations are avoided. In the planned deformation of the buffer housing, 10 to 20 times more energy is absorbed than in the standard actuation of conventional buffer springs.

This energy corresponds to a maximum impact speed for the railway vehicle of approximately 30 km/h, when equipped with EST crash buffers (fig. 5 and fig. 6). Under similar conditions, the maximum impact speed with conventional buffers is approximately 12 km/h.

Fig. 5 - *Deformable crash system in two stages type EST Duplex G1.A1*

Fig. 6 - *Deformable crash system in two stages type EST Duplex G2.A2*

By using these crash buffers, the following improvements in protection and safety can be achieved:

- faster recovery after accidents;
- reduction of repair costs after accidents;
- protection of personnel, passengers and goods;
- protection of all vehicles involved in a collision;
- avoiding uncontrolled collision scenarios (such as derailment), by initiating a less dangerous collision sequence;
- avoiding undetected damages as a result of moderate impacts.

The level of collision damage is quickly indicated using the witness marks on each buffer (fig. 7).

Fig. 7 - *Deformed crash buffer, type EST G1*

C. *AXTONE SA, Poland*

The Polish group AXTONE SA came into existence in 2007 in the small town of Kanczuga, through the merger of two companies, one German and the other Polish.

The AXTONE Group has a rich expertise in impact energy absorption for all types of railway vehicles. Buffers and passive crash protection elements, offered by AXTONE, ensure the safety of all vehicles in railway transport, as well as passengers or cargo transported.

AXTONE's innovative chipping technology consists of absorbing impact energy by permanently deforming a steel strip cut from the body of the buffer (fig. 8).

During a collision, the outer surface of the buffer shell is scraped by the chipping knives (fig. 9). The level of absorbed energy depends on the size and cross-sectional area of the resulting steel strip, which allows a wide adjustment of the parameters according to any application.

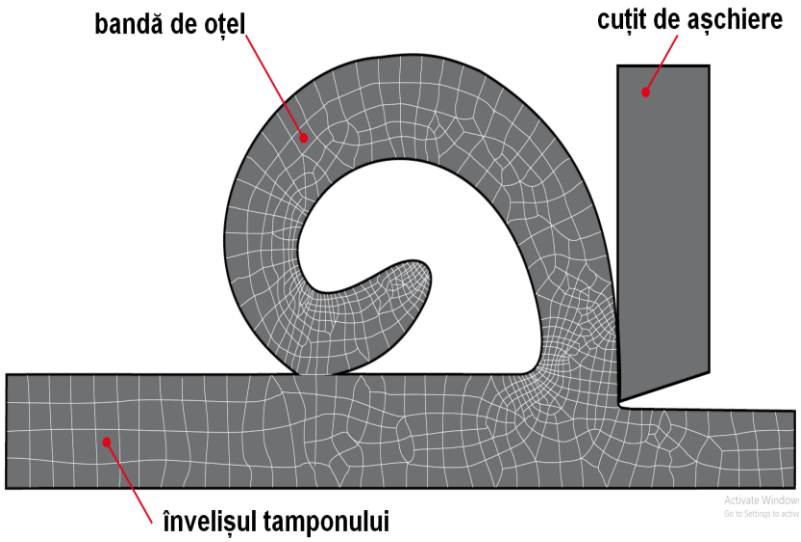

Fig. 8 - *Absorption of impact energy by chipping*

The main advantages of this solution include a low level of forces during collisions and stable operation. In addition, by increasing the cross-section, it is possible to increase the amount of absorbed energy according to the customer's needs. The weight of such a buffer is comparable to the weight of a type C buffer.

Fig. 9 - *Plastic deformed crash buffer by chipping*

The bending technology consists in absorbing the impact energy through the plastic deformation of the buffer sleeve, having the walls of a special shape (fig. 10). The level of absorbed energy depends on the deformation forces. By changing the shape of the sleeve, a wide range of controlled parameters is obtained, which can be modified in crash buffers according to individual customer requirements.

Fig.10 - *Crash buffer that uses the folding method to absorb impact energy*

Products manufactured in chipping technology can be used when free space is available behind the front cross-beam of the wagon. Buffers with folding technology do not require free space behind the front cross-beam of the wagon.

1.1.2. Research for the development of impact energy absorbing elements for railway vehicles

In the last 25 years, worldwide research in the field of impact energy absorption through the method of controlled plastic deformation, of some structural elements of railway vehicles, has experienced a permanent development, due to the particular increase in the volume of traffic and the speed of railway transport, on passenger and freight trains.

In the following, some of the most important studies conducted in the field and their main conclusions are presented in summary.

A. In 1999, Willibrordus J. Witteman, in his doctoral thesis, held at the Technical University of Eindhoven, on "Improving the impact resistance design of vehicles by controlling the energy absorbed in different collision situations", following the analysis of simulated models and collision tests performed on different metal profiles, reached the following conclusions:

- increasing the wall thickness of a profile increases the specific absorbed energy (per mass unit) more than increasing the perimeter of the profile;
- circular, hexagonal or octagonal profiles absorb a greater amount of energy through plastic deformation than square or rectangular profiles;

- the use of a trigger (through the controlled reduction of the resistance section of the profile) leads to the reduction of the maximum impact resistance force;

- among several types of triggers, reducing the thickness in the section by 10% provides a maximum of absorbed energy at impact.

Type of profiles used in tests:

Thickness = 2 mm;	Perimeter [mm]
A - square:	$300 = 4 \times 75$
B - rectangle:	$300 = 2 \times 60 + 2 \times 90$
C - circle:	$300 = \pi \times 95.5$
D - hexagon:	$300 = 6 \times 50$
E - octagon:	$300 = 4 \times 45 + 4 \times 30$

Properties of the steel used:

Young's modulus E = 210 kN/mm ^{2}

Yield strength σ_c = 185 N/mm ^{2}

Breaking strength σ_r = 325 N/mm ^{2}

Elongation at break A_5 = 47 %

(the material used has a high ductility)

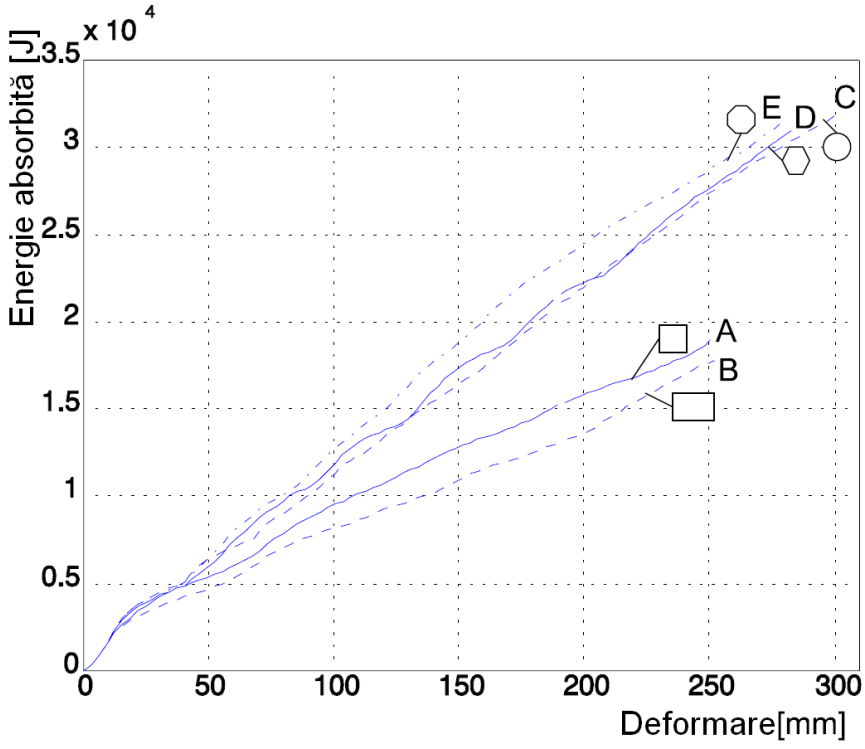

Fig. 11 - *Absorbed energy of five different profile types*

Figure 11 shows the graphical illustration of the dependence of absorbed energy as a function of strain value for a series of five different profile types.

Therefore, the circular (pipe) type profile is preferred both in terms of the level of specific energy absorbed and from the point of view of simplicity, symmetry and reduced manufacturing costs.

B. In 2007, M. Shakeri , S. Salehghaffari and R. Mirzaeifar , professors at the Mechanical Engineering Department of the Faculty of Technology in Tehran Polytechnic University, Iran, conducted a study on "Expansion of circular pipes with rigid pipes as energy absorbers of impact: theoretical and experimental research".

In this paper, the expansion of deformable tubes with the help of a rigid tube, under an axial compressive stress, represents a very effective process of absorbing impact energy (fig. 12). In this case, one of the pipes is considered rigid compared to the other, the materials from which they are made having different properties.

When this assembly is subjected to axial compression, the rigid pipe is inserted into the deformable one (fig. 13). Therefore, the impact energy is spent by the plastic expansion of the deformable pipe and the frictional energy between them (fig. 14).

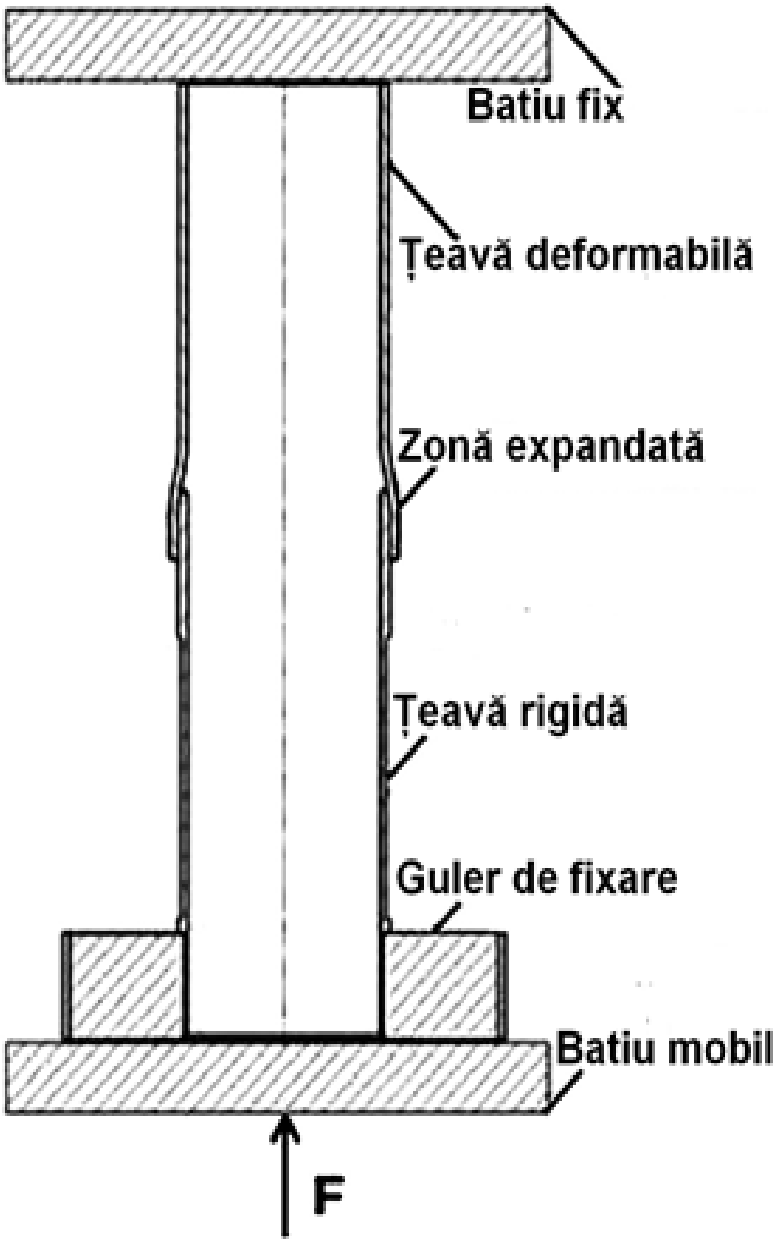

Fig. 12 - *Test sketch of the deformable assembly*

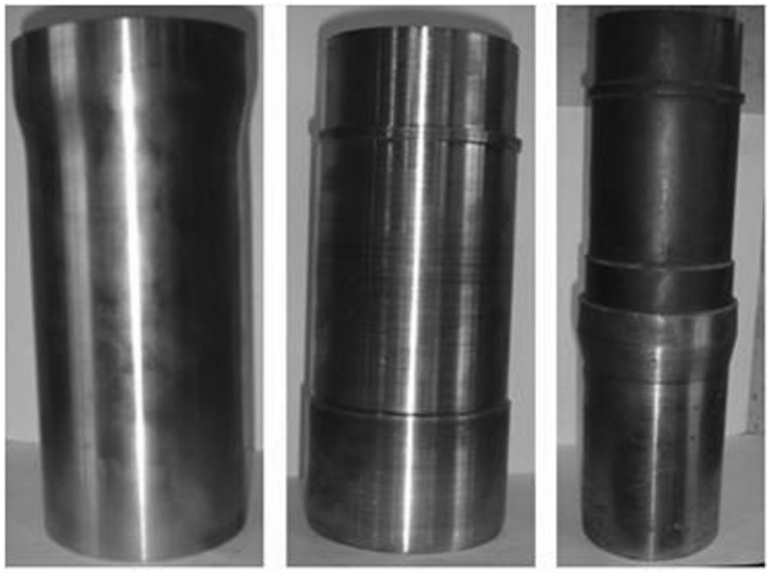

Fig. 13 - *Pipes used in the deformable assembly*
a - deformable pipe; b - rigid pipe; c - deformable assembly

The deformable pipe was made of S235 steel, had an initial inner diameter of 85 mm and a thickness of 3.5 mm. Both pipes used had the original length of 200 mm.

Fig. 14 - *Pipe assembly after deformation*

In this plastic deformation energy absorption mechanism, the average compressive force can be mainly influenced by the type of material, the thickness of the deformable pipe, the value of the coefficient of friction, and the value of the gap between the deformable pipe and the rigid pipe.

C. In 2007 and then in 2011, Jovan D. Tanasković , Dragan D. Milković and Vojkan J. Lučanin , professors of the Faculty of Mechanical Engineering at the University of Belgrade, Serbia, conducted studies on "Experimental Research of Kinetic Energy Absorbing Pipes during Collision" and "Experimental Determination and numerical of the characteristics of the collision energy absorption pipes".

The principle of energy absorption is based on the plastic deformation of a pipe, as a result of the reduction of its diameter when passing through a tapered ring, superimposed with the dissipation of energy through the friction between the pipe and the ring (fig. 15, fig. 16 and fig. 17). The pipe is made of steel type S235, and the ring of special high strength steel type C45E.

The tests carried out were both static and dynamic. The obtained results confirm that the force remains quasi-constant in both cases, throughout the movement, but the one in the dynamic test is about 20% higher than the one in the static test.

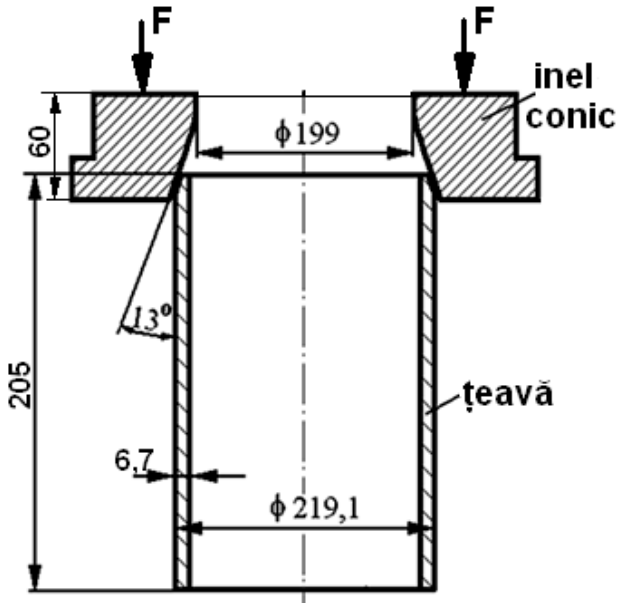

Fig. 15 - *Sketch of the energy absorbing device by the plastic deformation of the pipe*

Fig. 16 - *The device before plastic deformation of the pipe*

Fig. 17 - *The device after plastic deformation of the pipe*

Chapter 2

Qualitative-quantitative evaluations of impact energy absorption by the method of controlled plastic deformation of some structural elements of railway vehicles

2.1 Construction and collision resistance reference data of railway vehicles

2.1.1. General principles of passive structural safety in railway vehicles

Passive structural safety is the last means of collision protection, when all other possibilities to prevent an accident have failed. To protect passengers, train drivers, as well as dangerous goods, in the event of a railway accident, the following measures must be taken, in accordance with the requirements of the European standard EN 15227:2020, regarding the collision resistance of railway vehicles:

- absorption of impact energy in a controlled way;
- limiting the deceleration values (and the impact forces too);
- maintaining unaffected the survival space of the train drivers and the structural integrity of the areas occupied by passengers in the passenger carriages;
- reducing the risk of train collisions;
- reducing the risk of derailment when hitting an obstacle.

The first requirement will be analyzed in detail below, and regarding the second requirement, the maximum deceleration reached during the collision must not exceed by more than five times the acceleration gravity, to preserve the bodily integrity of the passengers.

Following the studies carried out, it is recommended, as an estimate of the deceleration duration, to choose the interval between the moment of impact and the moment when the interaction force drops to 10% of its maximum value.

2.1.2. Mass, speed and longitudinal compression resistance of railway vehicles

In order to be able to correctly evaluate the kinetic energy, therefore also the energy dissipated in the collision process of railway vehicles, we must determine, first of all, what are their tonnages and speeds.

In this sense, the main data regarding the railway vehicles used in Romania can be found summarized in the *"Regulation for the movement of trains and the maneuvering of railway vehicles - no. 005 of 26.10.2005"* and in the *"Towing and braking Regulation no. 006 of 26.10.2005"*, both with the latest changes from 30.10.2014 and published on the website of the Romanian Railway Authority - AFER.

Table 1 shows the masses and maximum speeds of the most representative railway vehicles in Romania:

Table 1 *- Masses and maximum speeds of different types of rail vehicles*

Type of railway vehicle	Maximum axle mass [tons]	Maximum total mass [tons]	Maximum travel speed [km/h]	
			Maneuver	Course
Electric locomotive	21,5	129	40	160
Diesel-electric locomotive	21,5	129	40	160
Diesel-hydraulic locomotive	17,5	70	40	100
Electric frame	17	68	40	120
Diesel car engine	18	72	40	120
Freight car	20	80	40	120
Passenger car	12,5	50	40	160

From the table above, the speed of 10 m/s = 36 km/h was selected for the calculations, which largely covers the maneuvering speeds, knowing that, in the last decades, among the railway accidents in Romania, resulting in head-on collisions, over 98% (according to the statistics of the Romanian Railway Investigation Agency - AGIFER) take place at speeds that do not exceed 36 km/h, on the lines diverted from stations, depots and railway yards.

As maximum masses, the variants of 130 t (heavy locomotives), 80 t (freight wagons), 70 t (light locomotives, diesel cars and electric frames) and 50 t (cars of passengers, metro or tram).

Thus, there can be a number of 16 combinations of collisions between different railway vehicles, one of which can be considered stationary and the other moving.

Regarding the maximum resistance to longitudinal compression of railway vehicles, they must bear compression forces of at least 2 MN, exerted on the front cross-beam of the chassis (symmetrically 1 MN on each buffer), so that the resistance structure does not suffer plastic deformations (leftovers).

2.1.3. Rail vehicle collision scenarios

Crash technology is a method of controlled transfer and absorption of a very high impact energy, in high-speed collision conditions. It was developed to increase the level of passive safety in rail transport.

The European standard EN 15227:2020 defines collision safety requirements for railway vehicles. The standard applies to various categories of railway vehicles, such as: locomotives, passenger trains (category CI), underground trains (category C-II), light trains (category C-III) and trams (category C-IV).

The collision scenarios described below do not represent the only cases of railway accidents encountered in reality, but they represent the most common collision situations that can result in victims:

A. Frontal impact between two identical railway vehicles; vehicles can belong to any of the four categories above.

B. Frontal impact between two different railway vehicles; those in category II and IV are excluded.

C. Frontal impact between a railway vehicle traveling at a traveling speed of no more than 110 km/h and a road vehicle with a large mass (15 t), located on a level crossing; category II and IV railway vehicles are excluded.

D. Frontal impact between a railway vehicle of category IV and a road vehicle of low mass (3 t); category I, II and III vehicles are excluded.

All scenarios assume the equipment of railway vehicles with crash buffers, which can absorb an impact energy of at least 400 kJ/piece.

In table 2, all combinations of collisions are presented synthetically, in accordance with the above scenarios, taking into account the masses and speeds of railway vehicles in Romania.

Table 2 *- Collision scenarios of different types of railway vehicles*

Fixed obstacle mass	Vehicles masses and speeds			
	130 t	80 t	70 t	50 t
130 t	10 m/s -15 m/s*	10 m/s -15 m/s*	10 m/s -15 m/s*	10 m/s -15 m/s*
80 t	10 m/s -15 m/s*	10 m/s -15 m/s*	10 m/s -15 m/s*	10 m/s -15 m/s*
70 t	10 m/s -15 m/s*	10 m/s -15 m/s*	10 m/s -15 m/s*	10 m/s -15 m/s*
50 t	10 m/s -15 m/s*	10 m/s -15 m/s*	10 m/s -15 m/s*	10 m/s -15 m/s*
15 t	10 m/s -15 m/s*	10 m/s -15 m/s*	10 m/s -15 m/s*	10 m/s -15 m/s*
	30 m/s	-	30 m/s	30 m/s
3 t	-	-	-	10 m/s -15 m/s*
	30 m/s	-	30 m/s	30 m/s

(*) The speed of 15 m/s = 54 km/h was taken into account following new studies carried out by the SNCF (French railway administration) and the Canadian industrial group Bombardier Transportation, under the direction of the UIC (International Union of Railways), of ERA (European Railway Agency) and of ERRI (European Railway Research Institute), within the SAFETRAIN research program, studies which argue, on statistical bases, the increase in the average speed at which collisions occur, along with the international development of the railway transport sector.

2.2 Preliminary requirements regarding impact energy absorbing elements for railway vehicles

2.2.1. Estimation of the impact energy absorbed in the collision of railway vehicles

Collisions between railway vehicles can be assimilated by simplification with the model of one-dimensional binary collisions, where the reaction energy **Q < 0** (endoenergetic), the collisions being inelastic (plastic, with energy absorption).

We are in the particular case where one of the bodies is at rest, and following the totally inelastic collision, the two bodies continue their movement together.

Thus, their speed after the collision will become:

$$v = \frac{m_1 v_1}{m_1 + m_2}$$

reaction energy Q (absorbed energy at impact) will be the following:

$$Q = \frac{m_1 m_2}{m_1 + m_2} \cdot \frac{v_1^2}{2}$$

It is also taken into account that, on each end of the railway vehicle, it will be possible to dissipate at most 2 x 0.5 MJ = 1 MJ of the total impact energy (through elastic + plastic deformation energy), with the help of two buffers of the crash type, among the best performing ones available worldwide, remaining dissipated like this:

Q ' = Q – 2 MJ (for two vehicles)

Q'' = Q – 1 MJ (for one vehicle)

In the ideal case, other forms of impact energy dissipation (thermal, gravitational field potential etc.) will be neglected, so that the entire remaining energy will be absorbed by the method of controlled plastic deformation of the protection elements (the most disadvantageous situation).

Taking into account the data from table 2, following the application of the calculation relations above, in table 3 we find synthesized the results for the speed of the group of vehicles and the energy dissipated after the collision.

From the analysis of the obtained results, it appears that, by absorbing an additional 1.1 MJ of energy per vehicle end (0.55 MJ per buffer), most of the collision cases in table 3 would be covered (especially the cases with a collision speed of 15 m/s), except those marked in red. The cases that are already covered, assuming the use of current crash pads, are marked in green. The cases that could be covered by using additional elements to absorb the impact energy are marked in blue.

***Table 3** - Energy dissipated after the collision*

Obstacle mass m_2		Vehicles masses and speeds							
		m_1 = 130 t		m_1 = 80 t		m_1 = 70 t		m_1 = 50 t	
$v_2 = 0$	v_1	10 m/s	15 m/s	10 m/s	15 m/s	10 m/s	15 m/s	10 m/s	15 m/s
130 t	v	*5m/s*	*7,5m/s*	*3,8m/s*	*5,7m/s*	*3,5m/s*	*5,3m/s*	*2,8m/s*	*4,2m/s*
	Q	*3,25MJ*	*7,31MJ*	*2,48MJ*	*5,58MJ*	*2,28MJ*	*5,13MJ*	*1,81MJ*	*4,07MJ*
80 t	v	*6,2m/s*	*9,3m/s*	*5m/s*	*7,5m/s*	*4,7m/s*	*7m/s*	*3,8m/s*	*5,8m/s*
	Q	*2,48MJ*	*5,58MJ*	*2MJ*	*4,5MJ*	*1,87MJ*	*4,21MJ*	*1,54MJ*	*3,47MJ*
70 t	v	*6,5m/s*	*9,8m/s*	*5,3m/s*	*8m/s*	*5m/s*	*7,5m/s*	*4,2m/s*	*6,3m/s*
	Q	*2,28MJ*	*5,13MJ*	*1,87MJ*	*4,21MJ*	*1,75MJ*	*3,94MJ*	*1,46MJ*	*3,29MJ*
50 t	v	*7,2m/s*	*10,8m/s*	*6,2m/s*	*9,2m/s*	*5,8m/s*	*8,8m/s*	*5m/s*	*7,5m/s*
	Q	*1,81MJ*	*4,07MJ*	*1,54MJ*	*3,47MJ*	*1,46MJ*	*3,29MJ*	*1,25MJ*	*2,81MJ*
3 t	v	-	-	-	-	-	-	*9,4m/s*	*14,2m/s*
	Q	-	-	-	-	-	-	*0,14MJ*	*0,32MJ*
15 t	v	*9m/s*	*13,4m/s*	*8,4m/s*	*12,6m/s*	*8,2m/s*	*12,4m/s*	*7,7m/s*	*11,5m/s*
	Q	*0,67MJ*	*1,51MJ*	*0,63MJ*	*1,42MJ*	*0,62MJ*	*1,40MJ*	*0,58MJ*	*1,31MJ*
	v_1	30 m/s		-		30 m/s		30 m/s	
	v	*26,9 m/s*		-		*24,7 m/s*		*23,1 m/s*	
	Q	*6,05 MJ*		-		*5,56 MJ*		*5,19 MJ*	
3 t	v	*29,3 m/s*		-		*28,8 m/s*		*28,3 m/s*	
	Q	*1,32 MJ*		-		*1,29 MJ*		*1,27 MJ*	

It should be noted that an increase of only 50% in the collision speed v_1 produces a 2.25 times increase in the impact energy Q.

The energy that would remain to be dissipated, after absorbing part of the impact energy, through the combined use of the current crash buffers and some additional elements, becomes:

Q ' = Q – 4.2 MJ (for two vehicles)

Q" = Q – 2.1 MJ (for a vehicle)

The maximum force that can be applied to the end of the wagon must not exceed 2.5 MN, i.e. 1.25 MN/buffer (we cannot exceed the value of 2 MN by more than 25% for reasons of structural strength, because the safety

coefficients in the design of these vehicles starts from a minimum of 1.3), but not to produce decelerations greater than 5 g = 50 m/ s ^{2} (so as not to affect the passengers). Thus, for a railway vehicle with a mass of 50 t, we have a maximum allowed deceleration of 50 m/s ^{2} (a = F/m).

To achieve the dissipated energy of 1.1 MJ, which translates into the mechanical work of the plastic deformation force of 2.5 MN, it should be maintained quasi-constant along the plastic deformation length of the absorbent element: ***l = 1.1 MJ / 2.5 MN = 0.44 m.***

2.2.2. Dimensioning of impact energy absorption elements and the calculation verification of their mechanical resistance

From the considerations presented in the previous subsection, it appears that the impact energy level will be very high. Therefore, a material will be needed that absorbs a large amount of energy through plastic deformation, preferably an unalloyed steel, with good plasticity (high tensile elongation) and good toughness (high resilience - high energy absorbed when bending through shock).

Steel, although it has a high specific weight compared to composite materials (in the present case the mass of the protective structural elements is estimated to be below 0.5% of the mass of the railway vehicle, its weight can be neglected), has the following advantages:

- well-known manufacturing technology and processing, with relatively low prices per mass unit;
- long lifespan, with minimal maintenance costs, comparable to the structures of railway vehicles (over 30 - 40 years);
- easy and low-cost implementation on old structures already in operation;
- easy recycling at the end of the life of the railway vehicle.

The structural element was chosen to be cylindrical in shape, because it presents a symmetry around the longitudinal axis, but also against all diametrical planes perpendicular to the bases, thus offering a good and equal resistance, due to symmetry. The creation of an energy absorption area from a set (matrix) of similar neighboring identical elements was considered, located on the front cross-beam of the wagons.

The aim was to find the most suitable dimensions for the outer diameter, wall thickness and cylinder height. The static compression stress was taken into account, so that the structure does not plastically deform in the cylindrical portion at forces lower than 2.5 MN or lose its stability through the buckling phenomenon. Plastic deformation at forces above 2.5 MN must occur only by increasing the diameter and obviously, by thinning the wall to the point of breaking, following the forced introduction in the vertical direction of a high-rigidity tapered element, made of high-strength alloy steel.

It was ensured that the elements in front of the front cross-beam do not deform plastically at the same time under compressive stresses of less than 2 MN (assuming a perpendicular stress uniformly distributed on all elements),

a condition imposed on the front cross-beam by the EN 12663-1/2015 standard. At the same time, these elements must undergo controlled plastic deformation at compressive stresses exceeding by more than 25% the limit of 2 MN, in order to protect the resistance structure of the railway vehicle chassis (safety coefficients in the design of railway vehicle structures start from 1,3).

Also, when choosing the material and dimensioning the elements, the manufacturing standard was taken into account and the typical dimensions for drawn pressure pipes EN 10216-1:2013 (not longitudinally welded on generators), so that pipes with the selected dimensions can be supplied by the rolled products industry.

According to the previous assumptions, the force from which the protective elements in front of the front cross-beam of the wagon should plastically deform is:

$$\boldsymbol{F = 1,25 \times 2\ MN = 2,5\ MN}$$

Taking into account the gauge restrictions imposed for the wagon, the maximum length of the assembly of protective elements cannot exceed 600 mm. Therefore, the total energy absorbed following their plastic deformation will be equal to the mechanical work of deformation:

$\boldsymbol{E = 2,5\ MN \times l = 1,1\ MJ}$, from where $\boldsymbol{l = 0.44\ m}$

Taking into account the fact that there will be a number of 10 identical elements, distributed symmetrically on the front cross-beam and that each will be equally stressed, then the compression force exerted on each element will be 250 kN, causing their plastic deformation through expansion.

In the following, a single element will be studied in isolation, assuming that the effects add up for all 10 elements. The arrangement of these elements is shown in figures 18 and 19, for one half of the front cross-beam, for reasons of symmetry.

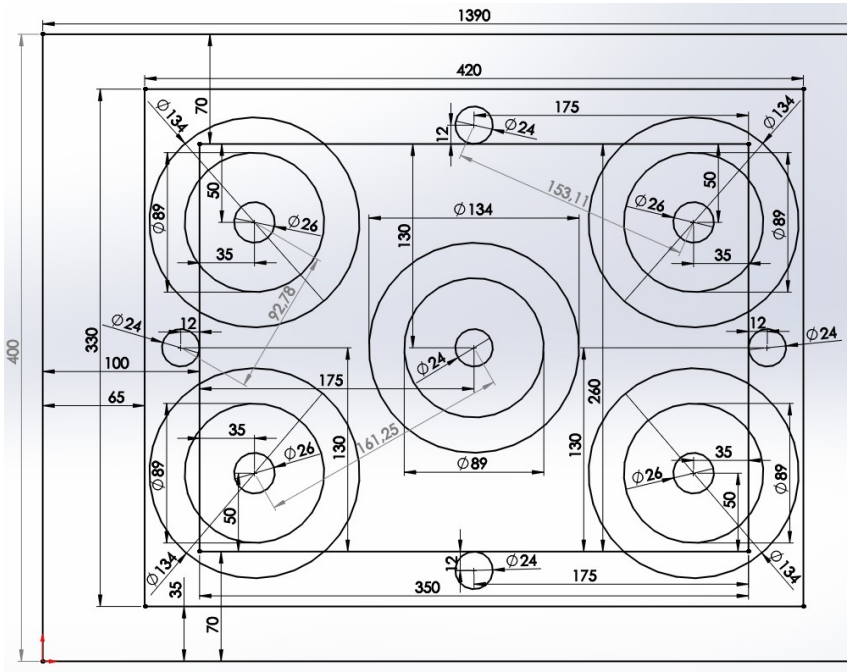

Fig. 18 - *Arrangement of energy absorption elements for half of the front cross-beam*

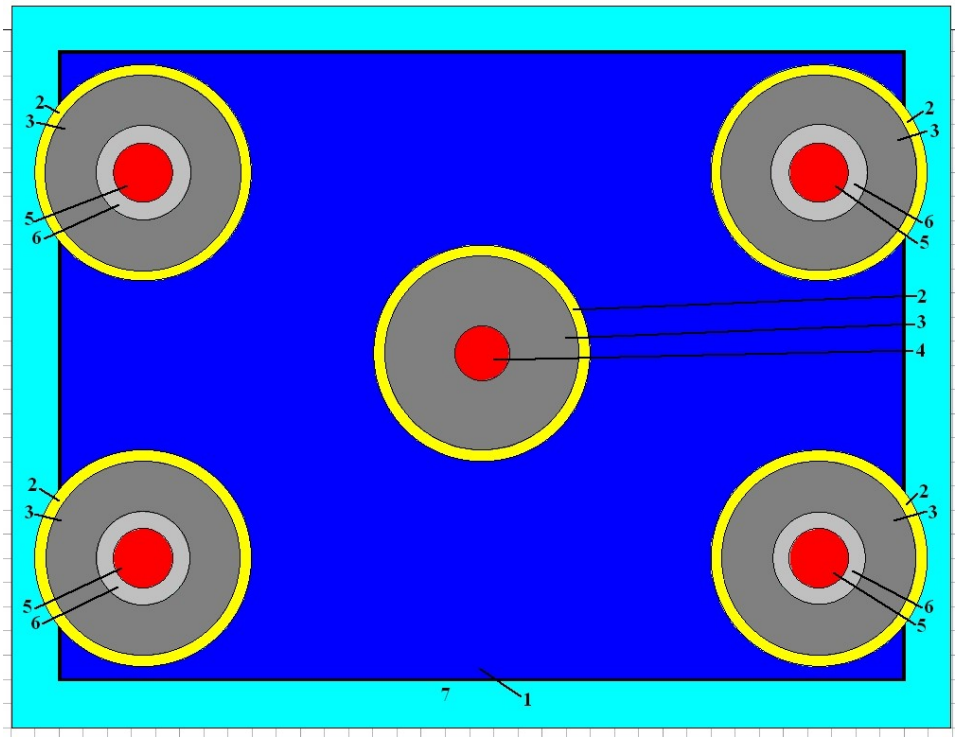

Fig. 19 - *Arrangement of energy absorbing elements under the buffer sole*

1 – The sole of the buffer

2 – Deformable pipe

3 – Guide flange (fig. 20)

4 – Fixing screw of the central guide flange

5 – Buffer fixing screw

6 – Elastic washer for fixing the guide flange

7 – Fixing plate

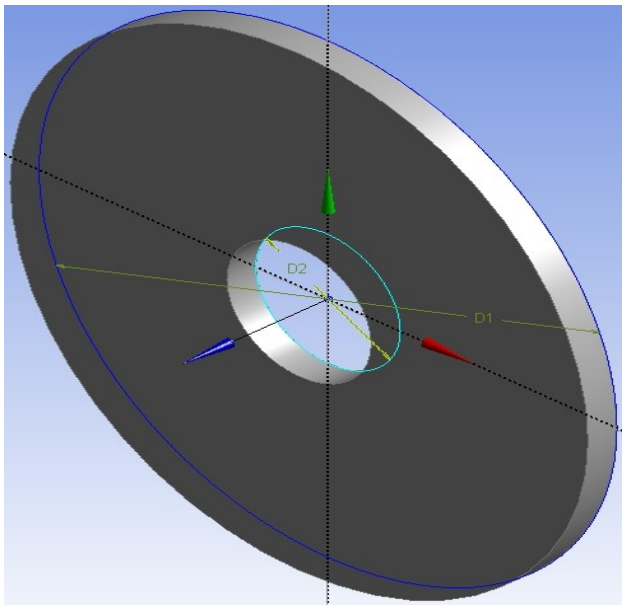

Fig. 20 - *Guide flange*

The outer diameter chosen for the pipe is 89 mm (3½”), with a wall thickness of 4 mm.

The resulting annular cross-section has an area of 1068 mm^2. Taking into account that a vertical force of 250 kN is exerted, a static compression stress of 234 MPa results.

The pipe has a fixed end, the other being deformable, by means of the tapered penetrator (tap type).

The entire assembly of structural energy absorbing elements will be fixed to the central cross-beam by means of steel plates tightened by four pre-tensioned 24 mm diameter, high strength (class 12.9) bolts , each capable of providing a maximum clamping force of over 400 kN .

Table 4 shows the main characteristics of the materials chosen to make the energy absorbing elements.

Table 4 - *Characteristics of the materials for the impact energy absorption elements*

Caracteristică material	Element	
	Penetrator tronconic	Țeavă cilindrică
Tip de oțel (marca)	45Cr2	S235JR
Modul de elasticitate	$1,9*10^5$ MPa	$2,1*10^5$ MPa
Coeficient Poisson	0,28	0,28
Densitate	7800 kg/m^3	7800 kg/m^3
Rezistența la rupere	780 MPa	360 MPa
Rezistența la limita de curgere	540 MPa	235 MPa
Alungirea relativă la rupere	min.12%	min.24%
Coeficient de dilatare termică	$1,1*10^{-5}$ /K	$1,1*10^{-5}$ /K
Conductibilitate termică	14 W/m/K	14 W/m/K
Căldură specifică	440 J/kg/K	440 J/kg/K
Energie de rupere la încovoiere prin șoc (K_v)	min. 35 J	min. 27 J

The tapered penetration element was designed with a tip angle of 60^0, after which its compression behavior was analyzed under a load of 250 kN, it could show only small deformations in the elastic range, due to the fact that the chosen material, 45Cr2, is a brand of high-strength alloy steel, having a breaking strength at least double that of the material from which the deformable elements are made.

Figure 21 shows the sketch of a longitudinal section of the energy absorbing assembly.

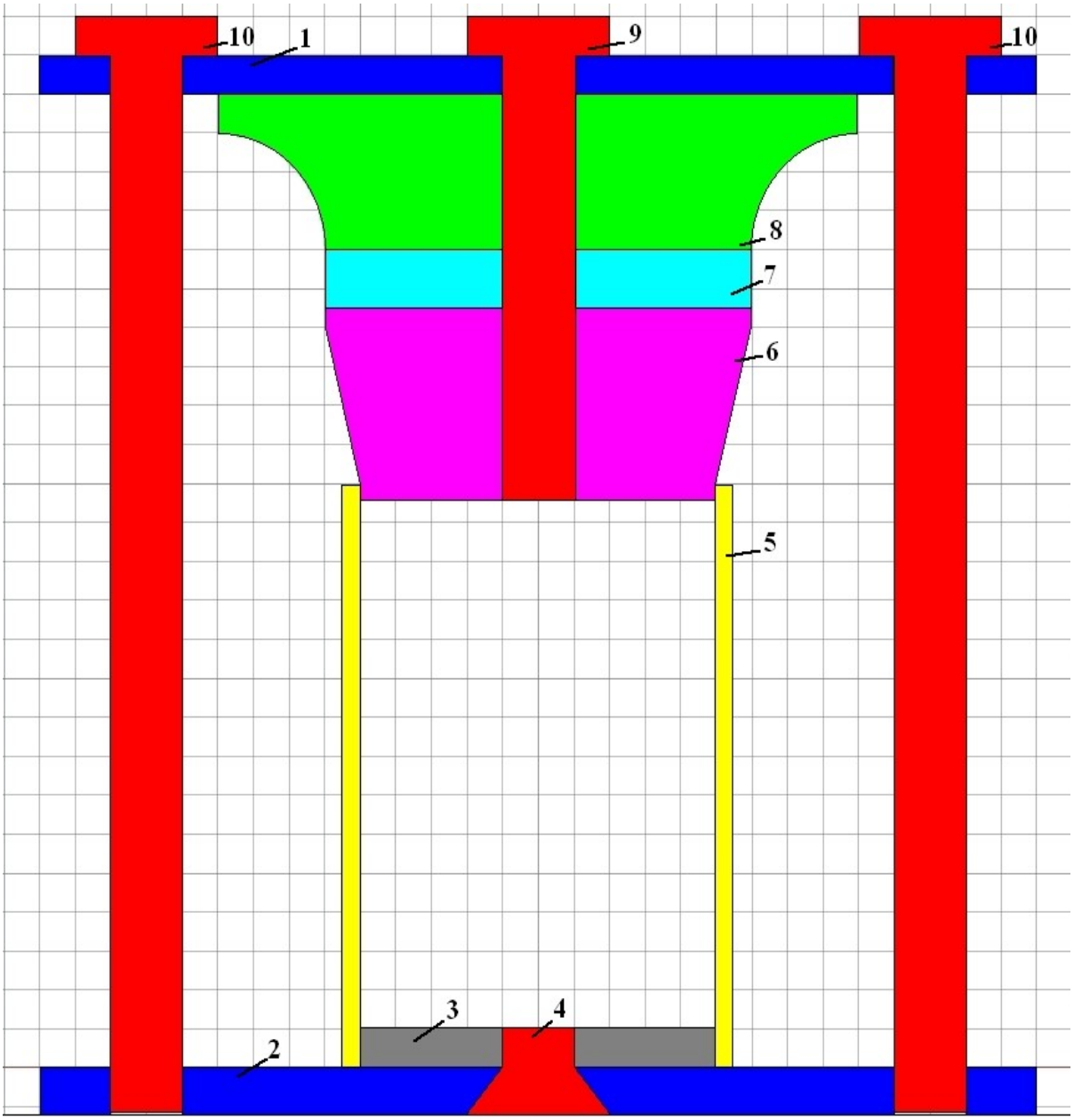

Fig. 21 - *Section through the energy absorbing assembly*

1 - The front cross member of the wagon
2 - Fixing plate of the penetrator assembly and the pad sole
3 - Cylindrical flange for guiding the deformable pipe
4 - Guide flange fixing screw
5 - Deformable pipe
6 - Truncated cone penetrator
7 - Chip support flange
8 - Flange for bending
9 - Fixing screw of the penetrator assembly
10 - Fixing screws by pre-tensioning the energy absorbing assembly

When dimensioning, it was considered that the variation of the inner diameter of the pipe should not exceed 25% (minimum elongation at break), so that the material of the pipe does not fail by breaking, upon reaching the maximum diameter of the penetrator.

The penetrator is made up of two cylinders of different radii, superimposed on a truncated cone, located in the middle, with an angle at the center of 60^0 and a generatrix length of 20 mm.

The connection was made using a radius of 5 mm between both cylindrical and tapered surfaces.

The lower cylindrical portion, having a radius of 40 mm and the height of 5 mm, serves to guide the tapered penetrator on the inside of the pipe.

Figure 22 shows a three-dimensional view of the penetrator.

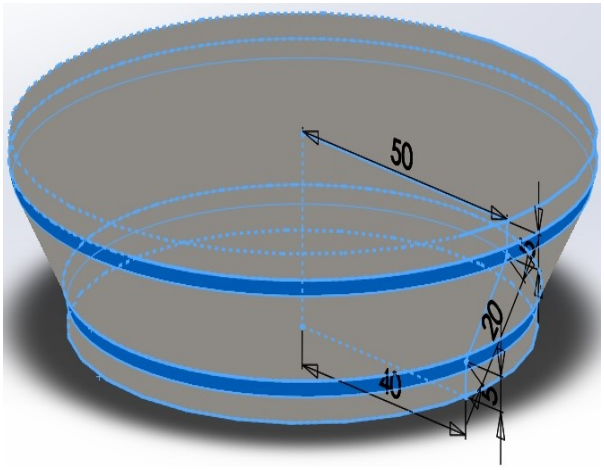

Fig. 22 - *Tapered penetrator*

Cylindrical flange chip support with a radius of 50 mm and the height of 10 mm, contains, uniformly distributed in the cross-section, at angles of 45^0 between them, eight chipping knives of width 3 mm, which exceed by 3 mm the maximum diameter of the penetrator (since after the expansion of the pipe, the wall thickness will be reduced from 4 mm to 3 mm) and which produce eight channels in the material of the expanded pipe, along eight generatrix, symmetrically positioned with respect to the longitudinal axis of the pipe, for the purpose of controlled reduction of the pipe section (fig. 24). Figure 23 shows a three-dimensional view of the bending flange, the last of the penetrator assembly.

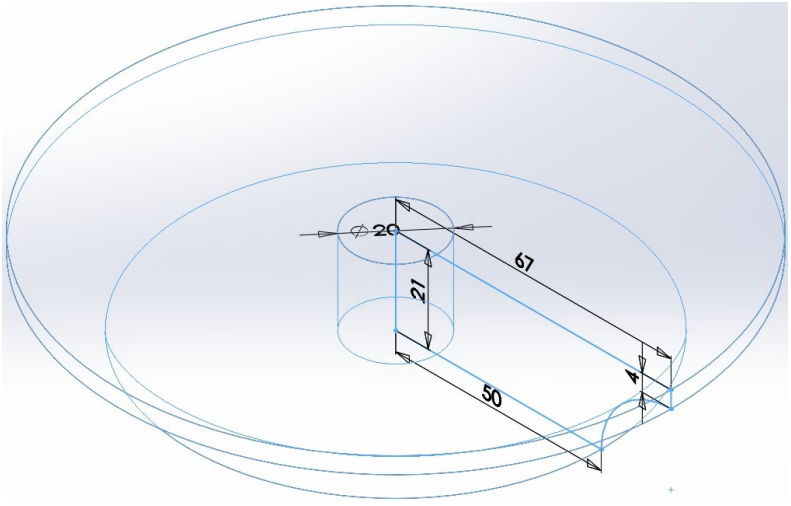

Fig. 23 - *Flange for bending*

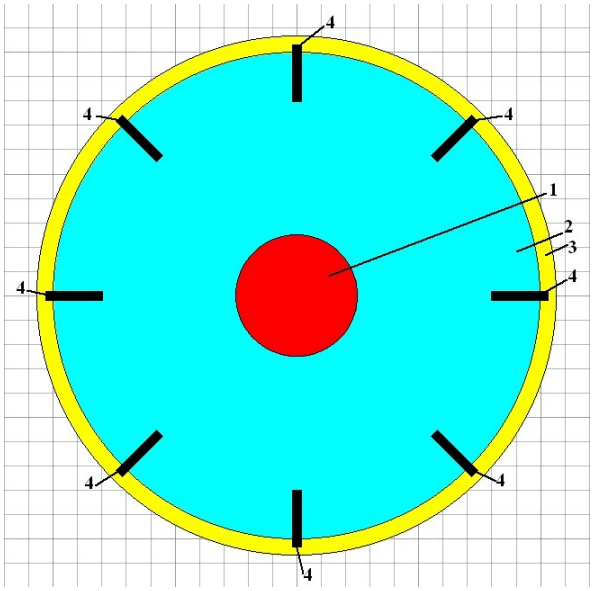

Fig. 24 - *Chip support flange*

1 - Fixing screw of the penetrator assembly
2 - Chip support flange
3 - Deformable pipe
4 - Eight chipping knives arranged symmetrically

Figure 25 shows the sketch of a longitudinal section of the energy absorbing assembly after the start of plastic deformation of the pipe.

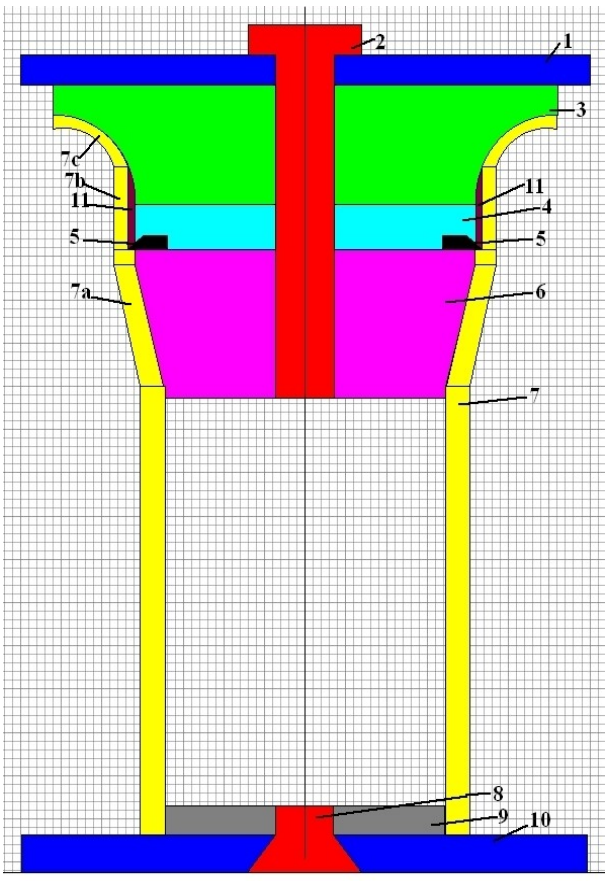

1 - The front cross-beam of the wagon
2 - Fixing screw of the penetrator assembly
3 - Flange for bending
4 - Chip support flange
5 - Chipping knives (width x depth = 3 x 3 mm)
6 - Tapered penetrator
7 - Undeformed pipe
7a - Expanded pipe
7b - Pipe with inner channel machined by chipping
7c - Pipe bent at 90^0 with a radius of 17 mm
8 - Guide flange fixing screw
9 - Cylindrical flange for guiding the deformable pipe
10 - Fixing plate of the penetrator assembly and the buffer sole
11 - Channels processed by chipping the deformable pipe body

Fig. 25 - *Section through the energy absorber assembly after pipe deformation*

The protective element was designed as a 600 mm long cylindrical pipe, with an inner radius of 40.5 mm and an outer radius of 44.5 mm.

Next, the stability of the cylindrical pipe element under the compression load was analyzed, in order to control its plastic deformation and to avoid buckling.

The slenderness coefficient of the bar will be calculated (for the selected steel, the minimum critical value is approximately 100 in the case of elastic buckling and approximately 60 in the case of plastic buckling):

$$\lambda = l_f \sqrt{\frac{A}{I_{min}}} \leq \pi \sqrt{\frac{E}{\sigma_f}} = 93{,}9$$

where l_f is the equivalent buckling length of the bar, σ_f is the critical buckling stress, E is the modulus of elasticity of the material, I_{min} is the minimum geometric moment of inertia (the buckling will occur in the plan where the section has a minimum moment of inertia), and A is the cross-sectional area of the bar:

$$A = \frac{\pi(D^2 - d^2)}{4} = 1068\ mm^2$$

where the outer diameter of the pipe is D = 89 mm, and the inner diameter of the pipe is d = 81 mm (the thickness of the pipe wall being 4 mm).

The equivalent buckling length of the bar depends on how its two ends are supported. In the case studied, it is a beam embedded at both ends:

$$l_f = l/2 = 300 \text{ mm}.$$

On the other hand, we have: E = 210000 N/mm^2, and at the limit:

$$\sigma_f = \sigma_c = 235 \text{ N/mm}^2$$

For the cross-section of the cylindrical pipe, the geometric moment of inertia is:

$$I = \frac{\pi(D^4 - d^4)}{64} = 966700\ mm^4$$

Entering the values in the definition relation, we obtain λ = 10, which means that no kind of buckling will occur, the pipe maintaining its stability.

2.2.3. Evaluation of impact energy absorption processes

Of the entire available free clearance of 600 mm, a portion of about 100 mm will be occupied by the guide flange with the fixing screws on the plate under the buffer sole.

Therefore, only a length of 500 mm can be considered as the active portion of the energy absorbing element.

On this length, under the action of a longitudinal force of no more than 2.5 MN on the end of the wagon, an energy of maximum 1.1 MJ (i.e. 110 kJ for each of the 10 elements) is intended to be absorbed.

A. Energy absorption by expanding the pipe by 25 %

Increasing the inner diameter by 25 % also implies increasing the pipe circumference by the same percentage over the length of 500 mm:

Δl_c = 0.25 x π x 89 mm = 69.9 mm

The area of the longitudinal section of the deformable pipe portion is:

A = 4 mm x 500 mm = 2000 mm^2

The force required at the breaking strength of the material will be:

$$F_m = A \times \sigma_r = 2000 \text{ mm}^2 \times 360 \text{ N/mm}^2 = 720 \text{ kN}$$

The mechanical work of expansion deformation will be:

$$L_e = F_m \times \Delta l_c = 720 \text{ kN} \times 69.9 \text{ mm} = 50.3 \text{ kJ}$$

B. Absorption of energy by friction of the surface of the tapered penetrator against the inner surface of the pipe

Taking into account the angle $\alpha = 30^0$ that the tapered surface makes with the vertical, the area of the tapered surface is:

$$A_t = \pi(D^2 - d^2)/4 \sin\alpha = 0.442d^2/\sin\alpha = 5800 \text{ mm}^2$$

However, there is the condition that, for the inside of a cylinder of diameter 81 mm and thickness s = 4 mm, the pressure exerted on the side walls of the pipe produces a tension in the material of the wall close to its breaking strength:

$$p_n = 2s\sigma_c/(d + s) = 33.9 \text{ N/mm}^2$$

The force exerted normal to the pipe wall will be:

$$F_n = p_n A_t = 196.5 \text{ kN}$$

According to the theory of molecular-mechanical friction, the frictional force has two components: a force for creating deformations and another for overcoming adhesions at the molecular level. The coefficient of friction (in the case of total plastic contact), has two components and is defined as follows:

$$\mu = (\tau_0 / \sigma_c + \beta) + k_p(p_n / \sigma_r)^{1/2} = (0.32 + 0.12) + 0.13 = 0.57$$

where $\tau_0 = 75$ MPa ; $\sigma_c = 235$ MPa ; $\sigma_r = 360$ MPa ; $\beta = 0.12$; $k_p = 0.55$

τ_0 = specific molecular resistance to material dissociation

β = piezo coefficient characteristic of the molecular component of friction

k_p = constant of the microgeometry (the shape of the roughness)

The frictional force will be:

$$F_f = \mu F_n = 112 \text{ kN}$$

The mechanical work of the frictional force will be:

$$L_f = F_f \times 0.5 \text{ m} = 56 \text{ kJ}$$

The total reaction force in the axial direction of the device will be:

$$R = F_n(\sin\alpha + \mu\cos\alpha) = 111.3 \text{ kN}$$

For the entire device containing 5 elements, the force will be 556.5 kN.

C. Energy absorption by chipping the pipe

In the case of chipping, we can consider that it is a shearing of the material in the area of action of the chipping knives. The section of the eight chipped channels is: $A_f = 8 \times 3 \text{ mm} \times 3 \text{ mm} = 72 \text{ mm}^2$

For ductile steels, it is estimated that: $\tau_f = 0.8\ \sigma_r$, so the force required for cutting will be: $F_a = A_f \times \tau_f = 20.7$ kN

Taking into account the length of the chipped portion of 470 mm (by subtracting the length of the penetrator from the 500 mm of the active portion), the mechanical work of chipping will be:

$$L_a = 9.7 \text{ kJ}$$

D. Energy absorption by bending pipe sections

Plastic bending involves stressing the material beyond its yield strength, along the entire path of plastic deformation.

The area of the eight sector sections of pipe thinned by 25 %, resulting from chipping, is:

$A_î = 1068\ mm^2 – A_f = 996\ mm^2$, i.e. for each section we have:

$A_î/8 = bh = 41.5\ mm \times 3\ mm = 124.5\ mm^2$ (b = width, h = thickness)

We consider the model of bar supported at both ends, having the above dimensions and bending length $l = r2^{1/2} = 24$ mm (the length of the chord of the circular arc of 90^0 with a radius of 17 mm), and $\sigma_î = \sigma_r$ (at the limit).

The force exerted for a section will be:

$F_î = 2bh^2\sigma_î/3l = 3.74$ kN

The mechanical work in bending for a portion of the section will be:

$L = F_îr(1 – 2^{1/2}/2) = 18.6$ J

In the 450 mm available for bending (by subtracting the length of the penetrator and the thickness of the cutting flange from the 550 mm of the active portion), there will be 18.75 such zones, multiplied eight times.

The total mechanical work on bending will be:

$L_î = L \times 8 \times 18.75 = 2.8$ kJ

E. Total energy absorbed by an element by various methods of controlling plastic deformation

By summing the mechanical work at points A, B, C and D, the total energy absorbed by an element is obtained following the use of the controlled plastic deformation method:

$E = L_î + L_a + L_f + L_e = 118.8$ kJ

It turns out that, for the five elements that behave identically, in the composition of an energy absorbing device, the total value of absorbed energy can reach about 594 kJ, about 8 % more than even the targeted value of 550 kJ on a single device.

2.3 Re-evaluation of the requirements regarding a new impact energy absorbing element for railway vehicles

2.3.1. The design of a new impact energy absorption element and its mechanical resistance calculation verification

The realization of the device for absorbing the impact energy through plastic deformation, an aspect that was presented previously, requires a good alignment of the five constituent elements for a single assembly, in order for their identical and symmetrical behavior. It is also necessary to repeat the same machining operations five times, which would consume quite a lot of time in the manufacturing process.

In order to simplify the realization and to eliminate these disadvantages, a new design solution of this device was imagined, the dimensional constraints not allowing the diameters of the 5 elements to be increased.

The chosen solution uses a single impact energy absorption element by plastic deformation, composed of a cylindrical pipe and a penetrator, but of increased dimensions to be able to dissipate the same amount of energy.

Obviously, the new device fits into the same dimensions, has the same cylindrical shape (chosen optimally in the previous chapter), the materials used are the same (with the advantages also listed in the previous chapter), and the impact energy is dissipated by the same three methods (expansion, chipping and bending). The same standardized conditions were imposed for the resistance structure of the railway vehicle, but also for the standardized dimensions for drawn pipes manufactured by the profile industry.

The aim was to find the most suitable dimensions for the outer diameter and the thickness of the cylinder wall. The static compression stress was taken into account, so that the structure does not plastically deform in the cylindrical portion at forces lower than 2.5 MN or lose its stability through the buckling phenomenon. Plastic deformation at forces above 2.5 MN must occur only by increasing the diameter and, obviously, by thinning the wall to the point of breaking, following the forced introduction in the vertical direction of a high-rigidity tapered element, made of high-strength alloy steel.

According to the previous assumptions, the force from which the protective element in front of the front cross member of the wagon should plastically deform is:

$$F = 1.25\ MN \times 2 = 2.5\ MN$$

Therefore, the total energy absorbed as a result of its plastic deformation will be equal to the mechanical work of deformation:

$$E = L = F \times l = 2.5\ MN \times l = 1.1\ MJ$$, from where $$l = 0.44\ m$$

The arrangement of this element is shown in figures 26 and 27, for one half of the front cross-beam, for reasons of symmetry.

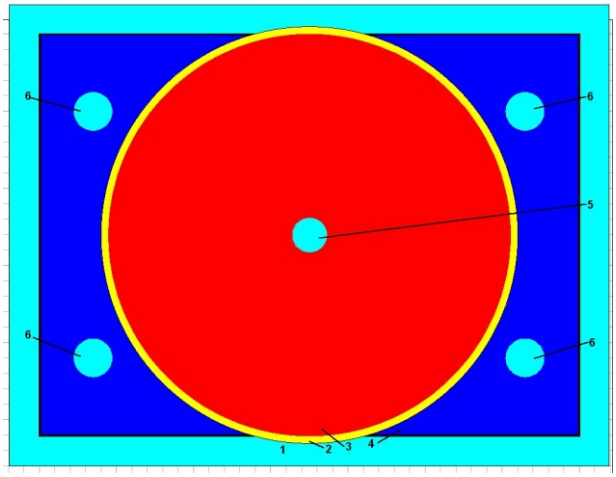

1 - Fixing plate on the front cross-beam
2 - Deformable pipe
3 - Guide flange
4 - Buffer sole
5 - Fixing hole of the central guide flange
6 - Buffer fixing holes

Fig. 26 - *The arrangement of the element of energy absorption under the sole of the buffer*

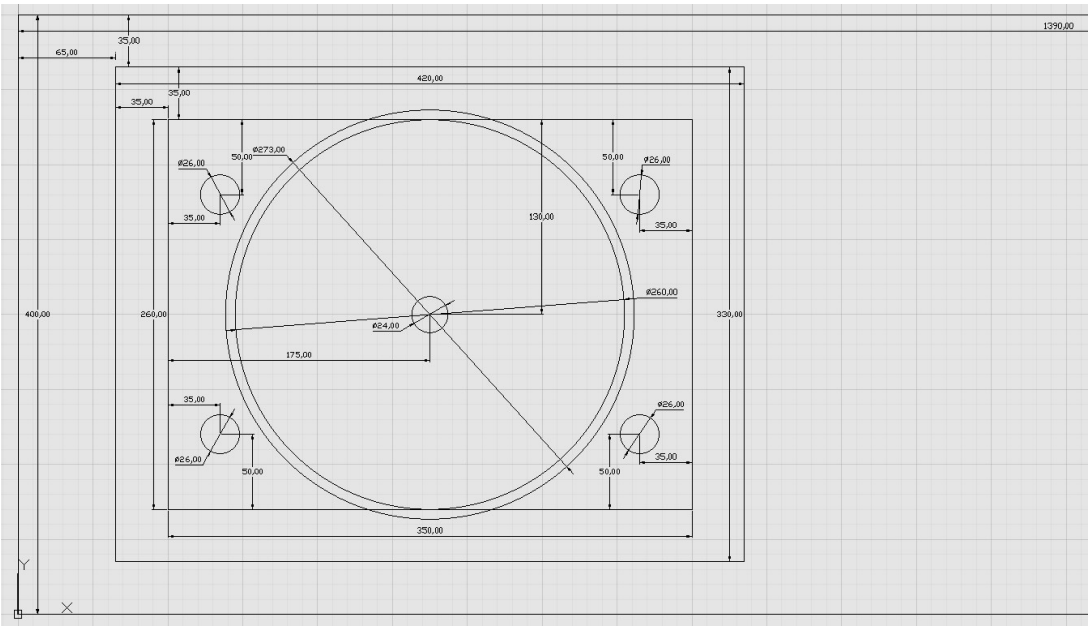

Fig. 27 - *Arrangement of the energy absorbing element for half of the front cross-beam*

The outer diameter chosen for the pipe is of 273 mm, with a wall thickness of 6.3 mm.

The resulting annular cross-section has an area of 5278 mm^2.

Taking into account that an axial force of 1250 kN is exerted, a static compression stress of 236.8 MPa results, very slightly above the minimum yield strength of 235 MPa.

The pipe has a fixed end, the other being deformable, by means of the tapered penetrator (tap type).

The entire assembly of energy absorbing elements will be fixed to the central cross member by means of four pre-tensioned steel plates of 24 mm diameter, high strength (class 12.9) bolts, each of which can provide a maximum clamping force of over 400 kN.

The tapered penetration element was designed with a tip angle of 60^0, after which its compression behavior was analyzed under a load of 1250 kN, it could present only small deformations in the elastic range, due to the fact that the chosen material, 45Cr2, is a brand of high-strength alloy steel, having a breaking strength at least double that of the material from which the deformable elements are made.

The frustoconical penetrator has a threaded central hole, 24 mm in diameter. When dimensioning, it was taken into account that the variation of the inner diameter of the pipe should not exceed 25 % (minimum elongation at break), so that the material of the pipe does not fail by breaking, upon reaching the maximum diameter of the penetrator of 322 mm.

The penetrator is made up of two cylinders of different radii, superimposed on a truncated cone, located in the middle, with an angle at the center of 60^0 and a generatrix length of 62 mm.

The lower cylindrical portion, having a radius of 130 mm and the height of 5 mm, serves to guide the tapered penetrator on the inside of the pipe.

Two three-dimensional views of the penetrator are shown in Figures 28 and 29.

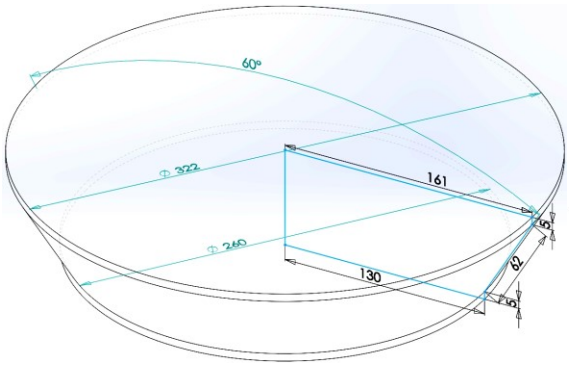

Fig. 28 - *Tapered penetrator without central hole*

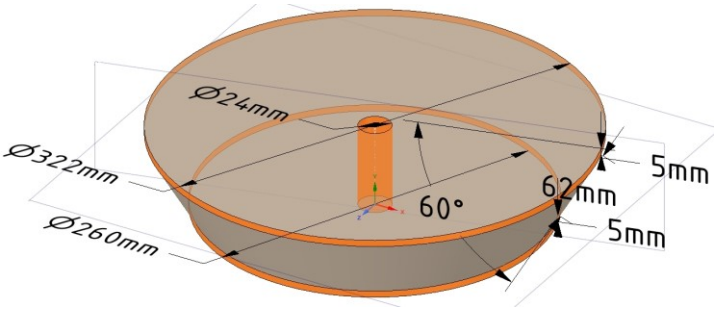

Fig. 29 - *Tapered penetrator with central hole*

Cylindrical flange support for chipping, having a radius of 161 mm and height 10 mm, contains, uniformly distributed in cross-section, at angles of 45^0 to each other, 8 or 12 chipping knives 6 mm wide, exceeding by 6 mm the maximum diameter of the penetrator and producing 8 or 12 channels in the material expanded pipes, along 8 generatrix, symmetrically positioned with respect to the longitudinal axis of the pipe, for the purpose of the controlled reduction of the pipe section (fig. 30).

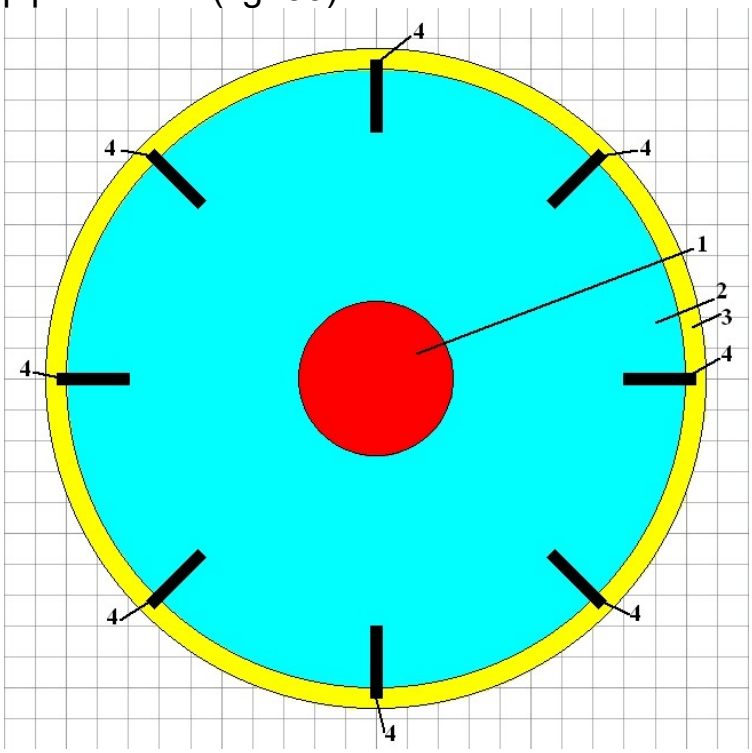

Fig. 30 - *Median cross-section through the chip support flange*

1 - Fixing screw of the penetrator assembly
2 - Chip support flange
3 - Deformable pipe
4 - Eight chipping knives arranged radially symmetrically (there can be 12 in another version of the device configuration)

Figure 31 shows a three-dimensional view of the bending flange, the last of the penetrator assembly.

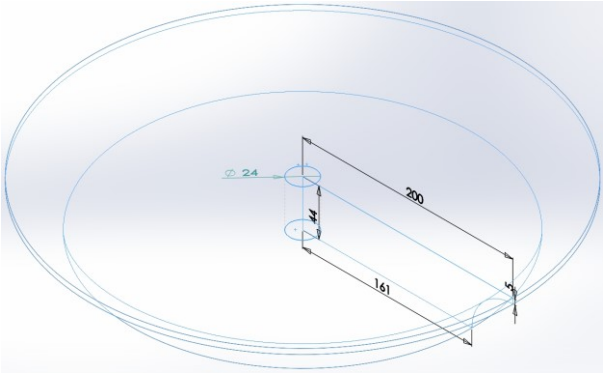

Fig. 31 - *Flange for bending*

Protective element was designed as a 600 mm long cylindrical pipe, with an inner diameter of 261 mm and an outer diameter of 273 mm.

Next, the stability of the cylindrical pipe element under the compression load was analyzed, in order to control its plastic deformation and to avoid buckling.

The slenderness coefficient of the bar was calculated (for the selected steel, the minimum critical value is approximately 100 in the case of elastic buckling and a minimum of 60 in the case of plastic buckling):

$$\lambda = l_f \sqrt{\frac{A}{I_{min}}} = \frac{4l_f}{\sqrt{D^2+d^2}} \leq \pi \sqrt{\frac{E}{\sigma_f}} = 93{,}9$$

where l_e is the equivalent buckling length of the bar, σ_f is the critical buckling stress, E is the modulus of elasticity of the material, I_{min} is the minimum geometric moment of inertia (the buckling will occur in the the plan where the section has a minimum moment of inertia), and A is the cross-sectional area of the cylindrical bar:

$$A = \frac{\pi(D^2-d^2)}{4} = 5278 \text{ mm}^2$$

The equivalent buckling length of the bar depends on how its two ends are supported.

In the case studied, it is a beam embedded at both ends:

$$l_f = l/2 = 300 \text{ mm}.$$

On the other hand, we have: $E = 210000$ N/mm^2, and at the limit:

$$\sigma_f = \sigma_c = 235 \text{ N/mm}^2$$

For the section cylindrical pipes, the geometric moment of inertia is:

$$I = \frac{\pi(D^4-d^4)}{64} = \frac{A(D^2+d^2)}{16}$$

Entering the values in the definition relation, we obtain $\lambda = 3.2$, which means that no buckling will occur in the pipe maintaining its stability.

2.3.2 Re-evaluation of impact energy absorption processes

Of the entire available free gauge of 600 mm, a portion of about 100 mm will be occupied by the guide flange with the fixing screws on the plate under the buffer sole.

Therefore, only a length of 500 mm can be considered as the active portion of the energy absorbing element.

On this length, under the action of a longitudinal force of no more than 2.5 MN per wagon end, a maximum energy of 1.1 MJ (i.e. 550 kJ for each energy-absorbing element) is intended to be absorbed.

A. Energy absorption by expanding the pipe by 25 %

Increasing the inner diameter by 25 % also implies increasing the pipe circumference by the same percentage over the length of 500 mm:

$$\Delta l_c = 0.25 \times \pi \times 273 \text{ mm} = 214.4 \text{ mm}$$

The area of the longitudinal section of the deformable pipe portion is:

$$A = 6.3 \text{ mm} \times 500 \text{ mm} = 3150 \text{ mm}^2$$

The force required at the breaking strength limit of the material will be:

$$F_m = A\sigma_r = 3150 \text{ mm}^2 \times 360 \text{ N/mm}^2 = 1134 \text{ kN}$$

The mechanical work of expansion deformation will be:

$$L_e = F_m \times \Delta l_c = 1134 \text{ kN} \times 214.4 \text{ mm} = 243.1 \text{ kJ}$$

B. Absorption of energy by friction of the tapered surface of the penetrator against the inner surface of the pipe

Taking into account the angle $\alpha = 30^0$ that the tapered surface makes with the vertical, the area of the tapered surface is:

$$A_t = \pi(D^2 - d^2)/4\sin\alpha = 0.442d^2/\sin\alpha = 60219 \text{ mm}^2$$

However, there is the condition that, for the inside of a cylinder of diameter 261 mm and thickness s = 6.3 mm, the pressure exerted on the side walls of the pipe produces a tension in the wall material close to its breaking strength:

$$p_n = 2s\sigma_r/(d + s) = 17 \text{ N/mm}^2$$

The force exerted normal to the pipe wall will be:

$$F_n = p_n A_t = 1023.7 \text{ kN}$$

According to the theory of molecular-mechanical friction, the friction force has two components: a force for making deformations and another for overcoming adhesions at the molecular level. The coefficient of friction (in the case of total plastic contact), has two components and is defined as follows:

$$\mu = (\tau_0 / \sigma_c + \beta) + k_p(p_n / \sigma_r)^{1/2} = (0.32 + 0.12) + 0.09 = 0.53$$

where $\tau_0 = 75$ MPa ; $\sigma_c = 235$ MPa ; $\sigma_r = 360$ MPa ; $\beta = 0.12$; $k_p = 0.55$

τ_0 = specific molecular resistance to material dissociation

β = piezo-coefficient characteristic of the molecular component of friction

k_p = constant of the microgeometry (the shape of the roughness)

The frictional force will be:

$$F_f = \mu F_n = 542.6 \text{ kN}$$

The mechanical work of the frictional force will be:

$$L_f = F_f \times 0.5 \text{ m} = 271.3 \text{ kJ}$$

The total reaction force in the axial direction of the device will be:

$$R = F_n(\sin\alpha + \mu\cos\alpha) = 981.7 \text{ kN}$$

C. Energy absorption by chipping the pipe

In the case of chipping, we can consider that we are dealing with a shearing of the material in the area of action of the chipping knives. Since we have a much larger circumference than in the first constructive solution, we can use 12 chipping knives.

The area of the section of the 12 chipped channels is:

$$A_f = 12 \times 6 \text{ mm} \times 6 \text{ mm} = 432 \text{ mm}^2$$

For ductile steels, it is estimated that: $\tau_f = 0.8\sigma_r$, so the force required for chipping will be: $F_a = A_f\tau_f = 124.4$ kN

Taking into account the length of the chipped portion of 430 mm (by subtracting the length of the penetrator from the 500 mm of the active portion), the mechanical work of chipping will be: $L_a = 53.5$ kJ

D. Energy absorption by bending pipe sections

Plastic bending involves stressing the material beyond its yield strength, along the entire path of plastic deformation.

The area of the 12 sector sections of pipe thinned by 25 %, resulting from chipping, is:

$$A_î = A - A_f = 5278 \text{ mm}^2 - 432 \text{ mm}^2 = 4846 \text{ mm}^2$$

that is, for each section we have:

$$A_î/12 = bh = 64.1 \text{ mm} \times 6.3 \text{ mm} = 403.8 \text{ mm}^2 \text{ (b = width, h = thickness)}$$

We consider the model of bar supported at both ends, having the above dimensions and bending length $l = r2^{1/2} = 55.2$ mm (the length of the chord of the circular arc of 90^0 with a radius of 39 mm), and $\sigma_î = \sigma_r$ (at the limit).

The force exerted for a section will be:

$$F_î = 2bh^2\sigma_î/3l = 11.1 \text{ kN}$$

The mechanical work in bending for a portion of the section will be:

$$L = F_îr(1 - 2^{1/2}/2) = 126.8 \text{ J}$$

In the 410 mm available for bending (by subtracting the length of the penetrator and the thickness of the cutting flange from the 500 mm of the active portion), we will have 7.4 such zones, multiplied by 12 times. The total mechanical work on bending will be: $L_î = L \times 12 \times 7.4 = 11.3$ kJ

E. The total energy absorbed by an element through various methods of controlling plastic deformation

By summing the mechanical work at points A, B, C and D, we will obtain the total energy absorbed by an element following the use of the controlled plastic deformation method:

$$E = L_î + L_a + L_f + L_e = 579.2 \text{ kJ}.$$

This proves that the value of 550 kJ of energy needed to be dissipated by a single element could even be exceeded by more than 5.3 %.

Chapter 3
Experimental validations of theoretical calculation methods of the impact energy absorption element on railway vehicles

3.1. Experimental validation of the theoretical method for calculating impact energies for two railway vehicles

3.1.1. Test conditions and measured parameters

To validate the theoretical collision energy calculation relationships (in the sense that energy losses due to other interactions can be neglected, such as axle bearing friction, wheel-rail contact friction or friction due to oscillations in bogie suspensions, all of which being much lower than the kinetic energies of the vehicles), the experimental results obtained during the collision tests carried out at the Făurei Railway Testing Center, belonging to the Romanian Railway Authority, were used.

The wagon made available for testing, the ZACS series (intended for the transportation of petroleum products), was fully equipped (fig. 32).

***Fig. 32** - ZACS series test car*

The characteristics of the tested wagon are as follows:

- length over buffers: 14940 mm;
- chassis length: 13700 mm;
- bogie wheelbase: 1800 mm;
- wagon wheelbase: 9400 mm;
- track gauge: 1435 mm;
- total tank capacity: 85 m^3;
- external diameter of the tank: 2950 mm;
- external length of the tank: 13000 mm;
- height of the axis of the pads at the level of the rail: 1060 mm;
- buffers category C, stroke 105 mm, maximum absorbed energy 75 kJ;
- bogie type: Y25 Cs ll-M;
- diameter of the rolling circle of the wheel: 920 mm;
- maximum axle load: 20 t;
- weight of the empty wagon: 23.4 t;
- mass of the full wagon: 79.6 t.

The data acquisition application was specially created for this project in the HBM Catman AP v5.2.2 program. Measuring equipment an HBM MX840B and MX1615B data acquisition system was used, along with a Panasonic laptop. The sampling frequency during the tests was 300 Hz.

Collision tests were initially done with the tank wagon empty, then loaded with water to full load, with it at rest, on a line in alignment and level. In fact, the moving wagon's speed is measured immediately before the collision, only after it arrives with both bogies on the alignment area and level landing (immediately to the left of the tested wagon), so that its movement is no longer accelerated by the descent on the inclined plane.

The two-bogie four-axle (high-walled but roofless) gondola-type moving wagon was loaded with crushed rock, having a total mass of 79.8 t. It was released freely from a line on an inclined plane. This wagon was fitted with the same type of category C buffers, stroke 105 mm, total absorbed energy minimum 75 kJ.

The reference document used was the standard SR EN 12663-2/2015 " Railway applications. Dimensioning requirements of railway vehicle structures. Part Two: Freight Wagons".

Collision speeds were between 4.2 m/s (15 km/h) and 2.2 m/s (8 km/h).

The speeds were determined based on the time elapsed between the time when the first axle of the first bogie of the moving wagon triggered the start of the track-mounted timer and the time when the second axle of the first bogie triggered the stop timer.

To reproduce the real situation, when the wagon transports petroleum products (having a lower density than water), and the liquid in the container is at a much higher level, the client used polyester anchored at the middle level of the container, by means of plastic nets attached with the help of metal elements welded directly to the container, in order to raise the center of gravity of the load.

Collision forces were measured with tensometric load cells, placed between the soles of the buffers and the front cross-beam. The prestress value was removed by an initial taring on each sample.

The stroke of the buffers was measured with inductive displacement transducers, located on the bodies of the buffers (fig. 33).

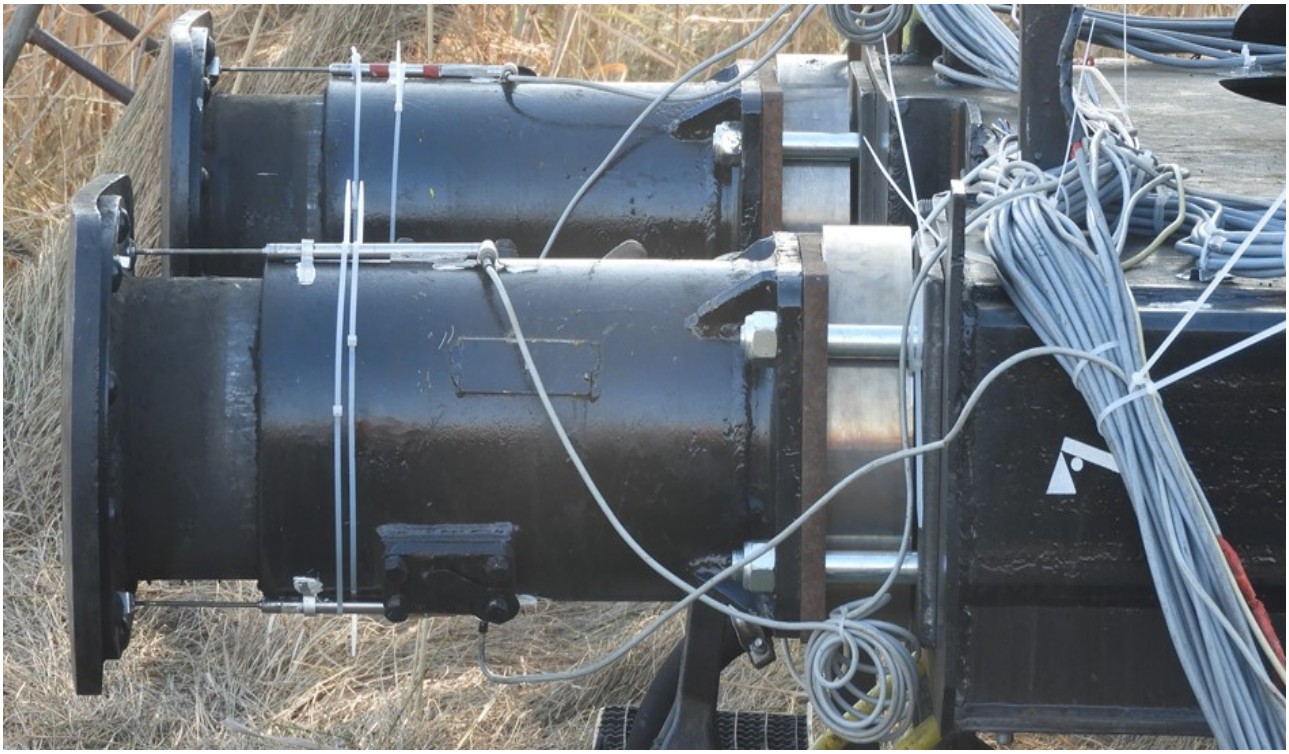

Fig. 33 *- Mounting the sensor assembly on the two buffers*

During these collisions, the evolution over time, for different collision speeds, of the following measured quantities was followed: the compressions of the buffers, the interaction forces at the level of the buffers, the movement speed of the assembly of the two wagons immediately after the collision and the deceleration (shock) of the tested wagon.

It should be remembered that the deformation (compression) of the buffers, although it was measured only on the tested wagon, is also symmetrical to the buffers on the moving wagon (according to the principle of action and reaction in mechanics), they being of the same type.

It can also be seen that the masses of the two loaded wagons were very close: the tested wagon had 79.6 t, and the moving one had 79.8 t. For this reason, to simplify the following calculations, we can approximate the two masses as equal to their average, i.e. 79.7 t.

The deceleration (shock) was measured using accelerometers mounted on the front cross-beam of the test wagon.

3.1.2. Verification of theoretical calculations by comparison with experimentally obtained results

By using the previous calculation relations, in which we use as input data the speed immediately before the collision of the buffer wagon (the tested

wagon being at rest) and the masses of the two wagons, we obtain the following theoretical results, summarized in table 5.

Table 5 *- Energy balance of collisions*

Mass of tested wagon [t]	Speed immediately before collision [m/s]	Kinetic energy before collision [MJ]	Reduced mass [t]	Energy absorbed [MJ]	Speed immediately after collision [m/s]	Kinetic energy after collision [MJ]
79,7	2	0,16	39,85	0,08	1	0,08
	2,1	0,18		0,09	1,05	0,09
	2,2	0,19		0,095	1,1	0,1
	2,3	0,21		0,105	1,15	0,11
	2,4	0,23		0,115	1,2	0,11
	2,5	0,25		0,125	1,25	0,12
	2,6	0,27		0,135	1,3	0,13
	2,7	0,29		0,145	1,35	0,15
	2,8	0,31		0,155	1,4	0,16
	2,9	0,34		0,17	1,45	0,17
	3	0,36		0,18	1,5	0,18
	3,1	0,38		0,19	1,55	0,19
	3,2	0,41		0,205	1,6	0,2
	3,3	0,43		0,215	1,65	0,22
	3,4	0,46		0,23	1,7	0,23
	3,5	0,49		0,245	1,75	0,24
	3,6	0,52		0,26	1,8	0,26
	3,7	0,55		0,275	1,85	0,27
	3,8	0,58		0,29	1,9	0,29
	3,9	0,61		0,305	1,95	0,3
	4	0,64		0,32	2	0,32
	4,1	0,67		0,335	2,05	0,33
	4,2	0,7		0,35	2,1	0,35

The collision test with the loaded wagon had the following main objectives:

- determining the maximum force behind both buffers on the test wagon;
- determining the compression of both buffers on the test wagon;
- determination of the maximum deceleration upon impact of the test wagon.

The velocity immediately before the collision was determined in two ways:

a. By the ratio between the wheelbase of the bogie (1.8 m) and the time recorded by the stopwatch (0.50 s), resulting in 3.6 m/s;

b. By analyzing the video images with a dedicated program, following the markings on the wheels and the angle made by them with a rectangular grid superimposed on the image, knowing that the rolling diameter of the wheels is 920 mm and the duration between two successive frames is 1/30 s; it was thus observed that an arc of a circle of 45^0 is traversed during three frames, so: $v = \pi D/0.8 = 3.61$ m/s.

In figure 34, the mark on the wheel in a vertical position is circled in red, and a and b denote the length of a buffer of 750 mm, respectively the distance between two successive crossbars of 750 mm (it turns out that between two adjacent points in the grid there are 250 mm at the level of the nearest rail).

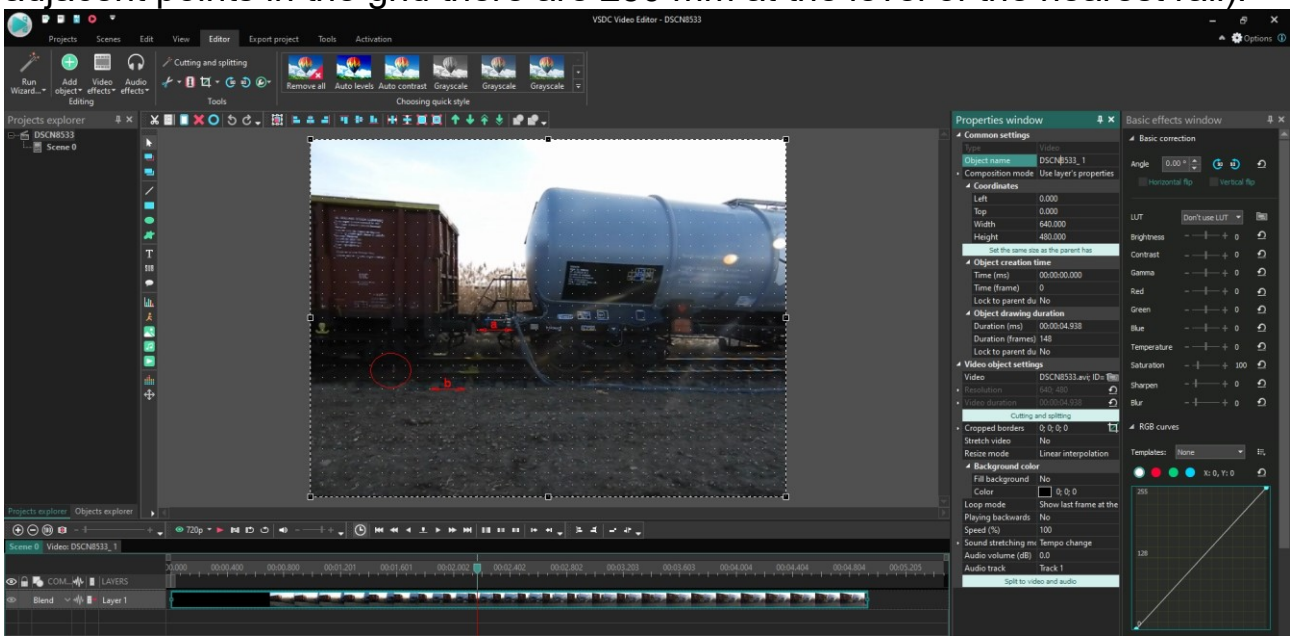

***Fig. 34** - Program dedicated to editing and analyzing video images*

It is noted that, by both methods of calculation, the same value of the speed was obtained, for which the speed immediately after the collision was also determined, by the second method (not having a second timer with a trigger/stop device mounted on the rail sole). Thus, a speed value of 1.8 m/s (half of the collision speed) was obtained, which was theoretically expected. The theoretically calculated energy dissipated in the collision will be in this case 260 kJ.

The maximum forces and compressions recorded on each of the two buffers averaged 1350.5 kN and 96 mm. The total mechanical work of elastic deformation (this is obtained by calculating the area under the F-d diagram for the buffer by the method of the smallest trapezoids - fig. 35), corresponding to the four identical buffers, is:

$$L = 4 \times 64.8 \text{ kJ} = 259.2 \text{ kJ}.$$

It is noted that the above value is less than the maximum for four buffers of 75 kJ each, i.e. 300 kJ.

The maximum deceleration measured was 34.15 m/s^2, i.e. 3.48 g.

The maximum deceleration, calculated for the maximum force applied to one end of the wagon, is: $a = 2F/m = 33.9$ m/s^2, i.e. 3.45 g.

Therefore, it is observed that the theoretical calculation model is validated by the experimental results obtained in the particular case of the presented collisions.

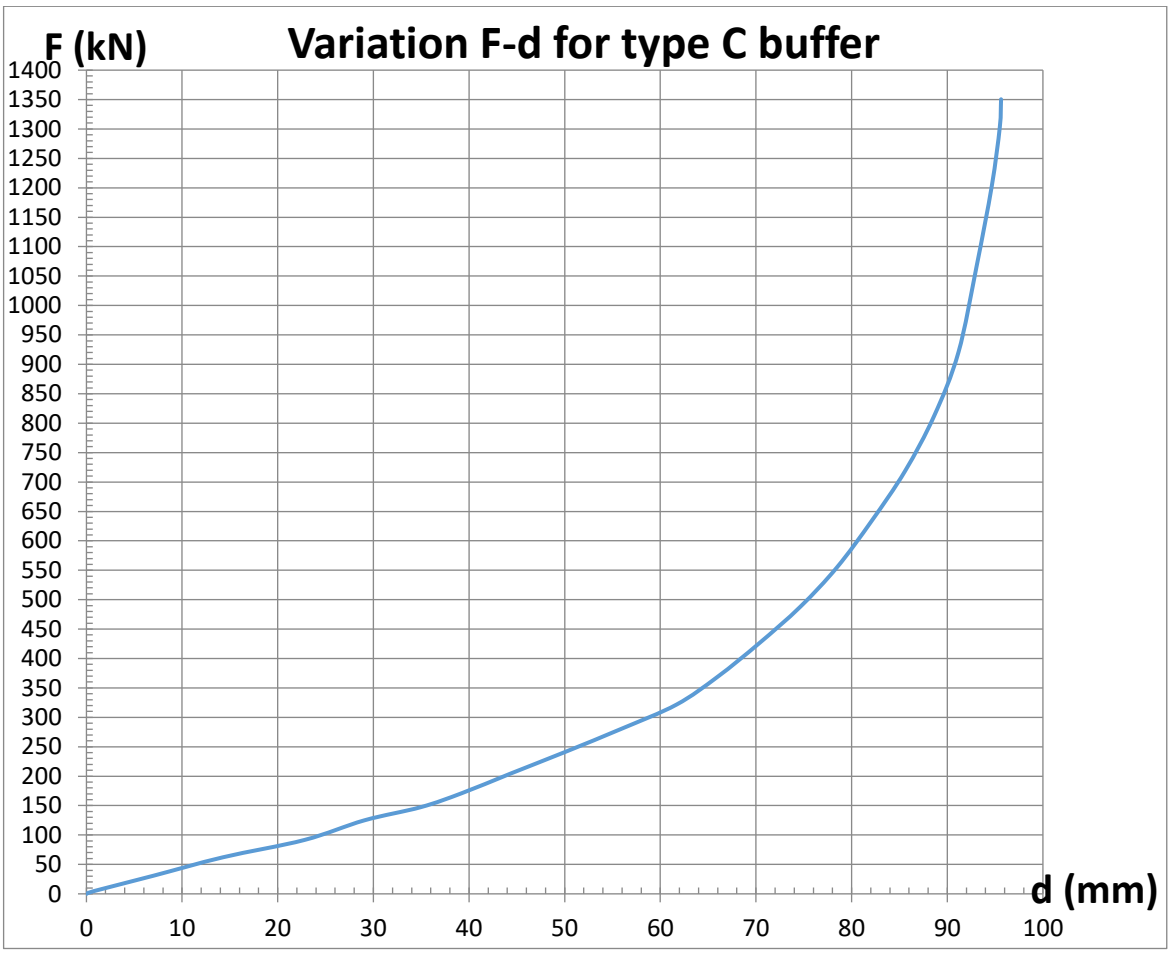

Fig. 35 *– F-d diagram for type C buffer*

3.2. Experimental validation of the theoretical calculation method for the axial compression stress of the impact energy absorption element by plastic deformation

3.2.1.Test conditions and measured parameters

In order to verify and validate the theoretical calculation method, used in the evaluation of energy absorbed by mechanical plastic deformation, following the axial compression, a static test of plastic deformation was carried out, in the laboratory of S.C. INNOVA SYSTEMS & TECHNOLOGIES S.R.L. from Arad. The test aimed to experimentally determine the values of the maximum forces reached in the case of controlled plastic deformation, for different angles of the penetrators used.

For this purpose, three cylindrical pipes were used, each 170 mm long, with an outer diameter of 133 mm and a wall thickness of 6 mm (an inner diameter of 121 mm).

The pipe had a cross-sectional area of 2394 mm^2, being of steel type S235JR, having a minimum yield strength of 235 N/mm^2 and a minimum elongation at break of 25 %, resulting in a minimum yield strength of 562.6 kN.

The penetrators were made of steel type S355JR, being made up of a cylinder, superimposed on a truncated cone, having the angles at the center of 60^0, 50^0 and 40^0.

The upper cylindrical portion had a height of 10 mm and a diameter of 152 mm (to satisfy the condition of a relative elongation of 25 % in the case of an inner diameter of 121 mm - fig. 35 and 36).

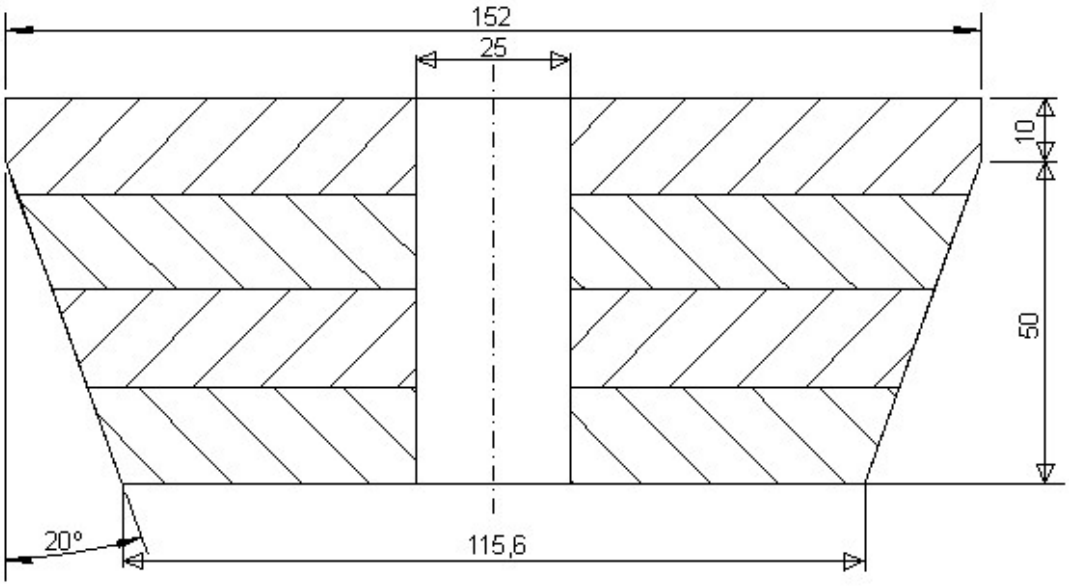

Fig. 35 *- Penetrator drawing with an angle at the center of 40^0*

Fig. 36 *- Penetrating body with an angle at the center of 40^0*

The test machine was a hydraulic press equipped with a 2 MN load cell, having four columns and a maximum stroke of 600 mm (fig. 37).

To measure displacement, the machine uses an inductive linear transducer and a computer system to acquire and process the recorded data.

Fig. 37 *- Test assembly on the hydraulic press*

The measurement chain also included a SPIDER 8 type signal amplifier from HBM (having eight input channels), to which the force and displacement transducers were connected. The software used was CATMAN from HBM, a dedicated program for the acquisition and processing of recorded data. A NIKON B600 ultrazoom compact camera was used for photography and video recording. The pipe deformation resulting from the test is shown in figure 38.

***Fig. 38** - Plastic deformation of the pipe after use of the penetrator with the tip angle of 40^0*

It was found that in the inlet end of the penetrator, the diameter of the pipe was slightly reduced, because the upper cylindrical part of the penetrator is not the same length as the pipe. During the test, the plastic deformation of the pipe was also accompanied by a massive release of heat, observed by increasing the local temperature of the pipe by more than 100^0C. After cooling, the free end of the pipe contracts more because it cools faster.

The reduction of the thickness of the pipe wall on the deformed portion was also observed, to a value of 4.5 mm, respectively by 25 % compared to the initial thickness of 6 mm. This is a normal fact, since the volume of material has remained the same. The penetrator (having a height of 50 mm) penetrated the inside of the pipe for a length of 120 mm, until it reached the lower support, i.e. the framing of the hydraulic press.

***Fig. 39** - Plastic deformation of the pipe after use of the penetrator with the tip angle of 50^0*

The tests carried out for the other two penetrators with the angles of 50^0 and 60^0 were not completed, because significantly exceeding the minimum yield strength generated the loss of stability of the pipe walls on one side (fig.39). The tests were immediately stopped, to avoid a possible accident due to the uncontrolled and extremely rapid spreading of the overlapping intermediate bodies for the application of the compressive force.

In these two cases, there was no need to redo the theoretical calculations for the given pipe and compare them with the experimental results, because they are not relevant.

3.2.2. Verification of theoretical calculations by comparison with experimental results for the deformed pipe with a penetrator having the center angle of 40^0

Figures 40, 41 and 42 graphically show the results of the controlled type plastic deformation test, by the axial compression stress of the pipe with the help of a penetrator with a tip angle of 40^0.

From the diagram d-t (fig. 40) it appears that the advance speed of the press was kept constant at the value of about 4 mm/s. For this reason, the diagrams F-t (fig. 41) and F-d (fig. 42) are similar.

From the F-d plot it appears that the maximum force reached was 600.7 kN and the average force (from 170 consecutive values) over the last 17 seconds of the test (when it can be considered to have reached a plateau) was 591.5 kN, which exceeds by only 5 % the minimum yield force of 562.6 kN (calculated in the previous subsection), the pipe remaining stable until the end of the test. The length of the plateau was 63 mm.

In conclusion, in this case it is necessary to redo the theoretical calculations for the given pipe and to compare them with the experimental results, the penetrator having the angle at the center of 40^0 being appropriate to the solution found, the penetration depth being of 120 mm.

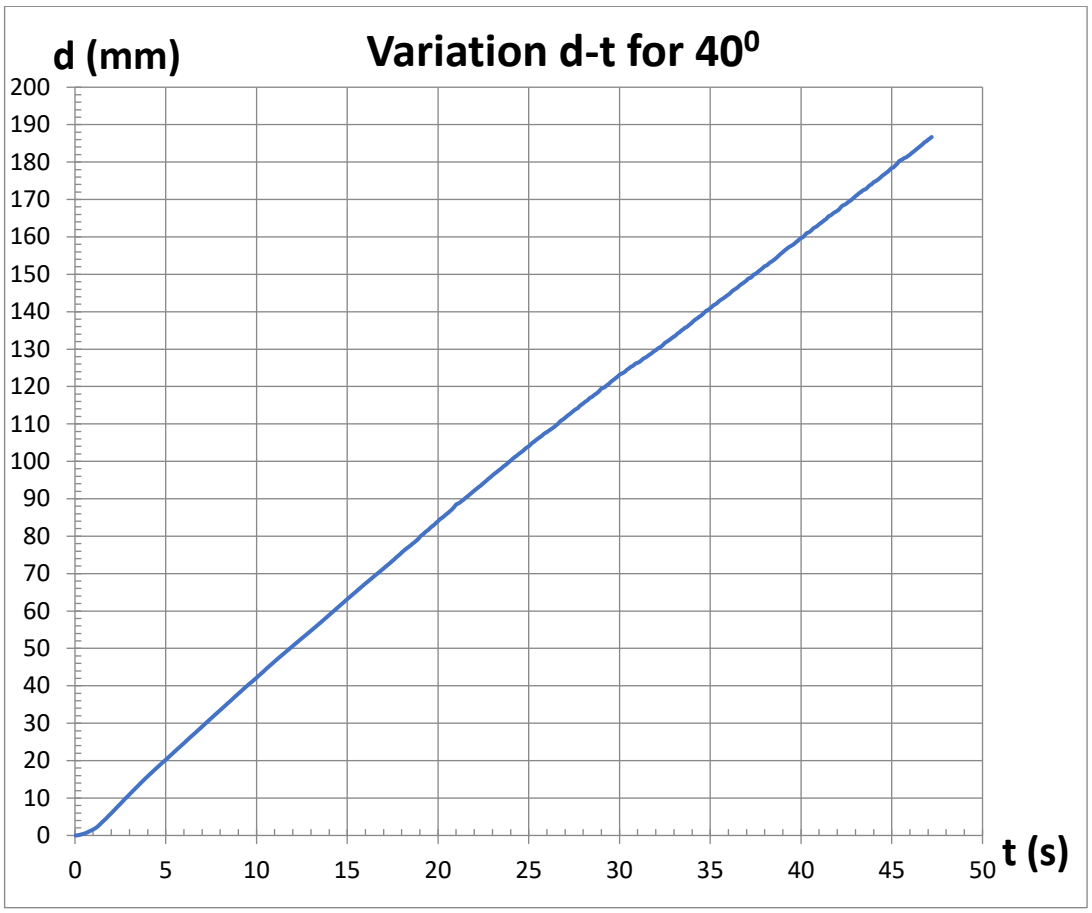

Fig. 40 *- Diagram d-t for 40⁰*

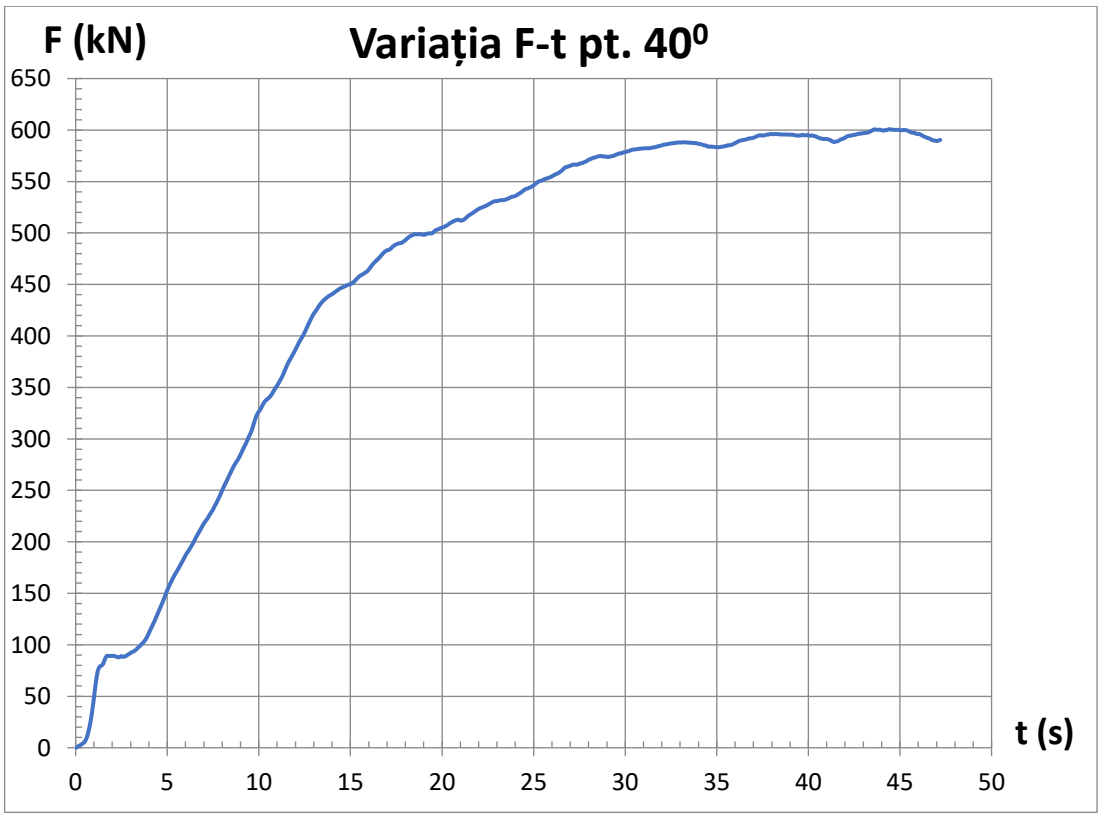

Fig. 41 *- Diagram F-t for 40⁰*

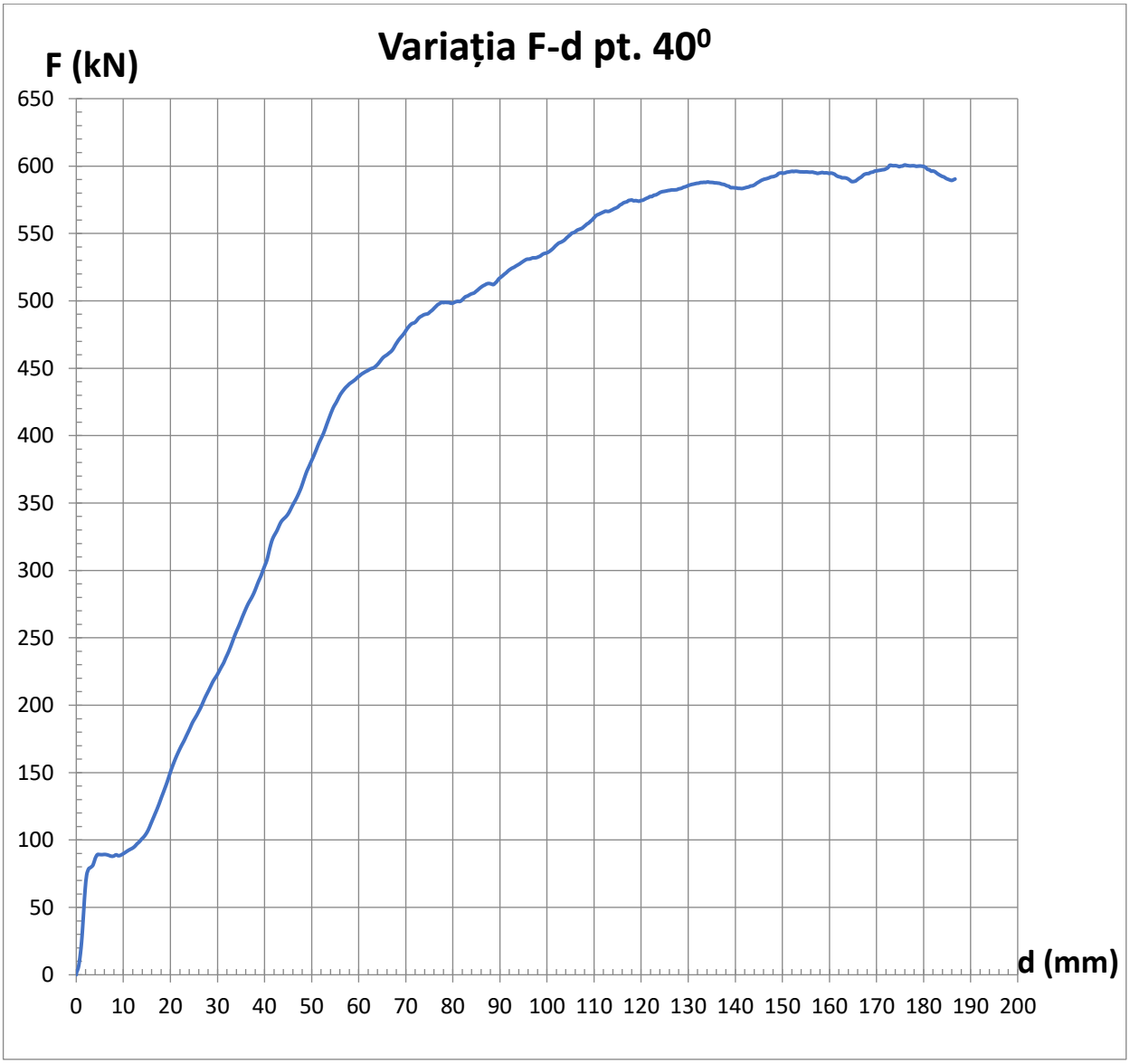

***Fig. 42** - Diagram F-d for 40⁰*

In order to validate the analytical calculation method, the results obtained experimentally for the maximum force and mechanical work of plastic deformation were compared with those obtained by analytical calculation.

Thus, the average value of the vertical compressive force was obtained as being 591.5 kN, along a plateau of 63 mm length. Therefore, the mechanical work over this distance required for the controlled plastic deformation of the pipe was 37.3 kJ.

It should be noted that the mechanical work served only the two physical processes involved on this section of the pipe: the expansion of the pipe and the friction of the tapered surface of the penetrator against the inner surface of the pipe.

Next, the same analytical calculation method was applied for the two physical processes, starting from the pipe parameters used in the experiment.

In this case, the total mechanical work was made up of only the two components mentioned above.

A. Energy absorption by expanding the pipe by 25 %

Increasing the inner diameter by 25 % also implies increasing the pipe circumference by the same percentage:

$$\Delta l_c = 0.25 \times \pi \times 133 \text{ mm} = 104.5 \text{ mm}$$

The area of the longitudinal section of the deformable pipe portion is (for the plateau portion only):

$$A = 6 \text{ mm} \times 63 \text{ mm} = 378 \text{ mm}^2$$

The force required at the breaking strength limit of the material will be:

$$F_m = A \times \sigma_c = 378 \text{ mm}^2 \times 360 \text{ N/mm}^2 = 136.1 \text{ kN}$$

The mechanical work of expansion deformation will be:

$$L_e = F_m \times \Delta l_c = 14.2 \text{ kJ}.$$

B. Absorption of energy by friction of the tapered surface of the penetrator against the inner surface of the pipe

Taking into account the angle $\alpha = 20^0$ that the tapered surface makes with the vertical, the area of the tapered surface is:

$$A_t = \pi(D^2 - d^2)/4\sin\alpha = 0.442d^2/\sin\alpha = 18921 \text{ mm}^2$$

However, we have the condition that, for the inside of a cylinder with a diameter of 121 mm and thickness s = 6 mm, the pressure exerted on the side walls of the pipe produces a tension in the material of the wall close to its breaking strength: $p_n = 2s\sigma_r/(d + s) = 34 \text{ N/mm}^2$

The force exerted normal to the pipe wall will be:

$$F_n = p_n A_t = 643.3 \text{ kN}$$

According to the theory of molecular-mechanical friction, the friction force has two components: a force for making deformations and another for overcoming adhesions at the molecular level. The coefficient of friction (in the case of total plastic contact), has two components and is defined as follows:

$$\mu = (\tau_0 / \sigma_c + \beta) + k_p(p_n / \sigma_r)^{1/2} = (0.32 + 0.12) + 0.13 = 0.57$$

where $\tau_0 = 75$ MPa ; $\sigma_c = 235$ MPa ; $\sigma_r = 360$ MPa ; $\beta = 0.12$; $k_p = 0.55$

τ_0 = specific molecular resistance to material dissociation

β = piezo coefficient characteristic of the molecular component of friction

k_p = constant of the microgeometry (the shape of the roughness)

The frictional force will be:

$$F_f = \mu F_n = 366.7 \text{ kN}$$

The mechanical work of the frictional force will be:

$$L_f = F_f \times 0.063 \text{ m} = 23.1 \text{ kJ}$$

The total reaction force in the axial direction of the device will be:

$$R = F_n(\sin\alpha + \mu\cos\alpha) = 564.6 \text{ kN}$$

In this case, the total mechanical work will be: $L_t = L_e + L_f = 37.3$ kJ.

Comparing the calculated value for R with the one obtained experimentally, it is found that the relative difference between the two values is less than 4.8%.

Moreover, it is observed that the value of the mechanical work of R on the 63 mm of the plateau is 35.6 kJ, i.e. still 4.8% less than L_t.

Following the findings above, it is necessary to reevaluate the analytical calculation model of the impact energy absorption element on a real scale, taking into account the angle $\alpha = 20^0$ that the tapered surface of the penetrator makes with the vertical.

A. Energy absorption by expanding the pipe by 25 %

Increasing the inner diameter by 25 % also implies increasing the pipe circumference by the same percentage over the length of 500 mm:

$$\Delta l_c = 0.25 \times \pi \times 273 \text{ mm} = 214.4 \text{ mm}$$

The area of the longitudinal section of the deformable pipe portion is:

$$A = 6.3 \text{ mm} \times 500 \text{ mm} = 3150 \text{ mm}^2$$

The force required at the breaking strength limit of the material will be:

$$F_m = A\sigma_r = 3150 \text{ mm}^2 \times 360 \text{ N/mm}^2 = 1134 \text{ kN}$$

The mechanical work of expansion deformation will be:

$$L_e = F_m \times \Delta l_c = 1134 \text{ kN} \times 214.4 \text{ mm} = 243.1 \text{ kJ}.$$

B. Absorption of energy by friction of the tapered surface of the penetrator against the inner surface of the pipe

Taking into account the angle $\alpha = 20^0$ that the tapered surface makes with the vertical, the area of the tapered surface is:

$$A_t = \pi(D^2 - d^2)/4\sin\alpha = 0.442d^2/\sin\alpha = 88034 \text{ mm}^2$$

However, we have the condition that, for the inside of a cylinder of diameter 261 mm and thickness s = 6.3 mm, the pressure exerted on the side walls of the pipe produces a tension in the material of the wall close to its breaking strength: $p_n = 2s\sigma_r/(d + s) = 17 \text{ N/mm}^2$

The force exerted normal to the pipe wall will be: $F_n = p_n A_t = 1496.6 \text{ kN}$

According to the theory of molecular-mechanical friction, the friction force has two components: a force for making deformations and another for overcoming adhesions at the molecular level. The coefficient of friction (in the case of total plastic contact), has two components and is defined as follows:

$$\mu = (\tau_0 / \sigma_c + \beta) + k_p(p_n / \sigma_r)^{1/2} = (0.32 + 0.12) + 0.09 = 0.53$$

where $\tau_0 = 75$ MPa ; $\sigma_c = 235$ MPa ; $\sigma_r = 360$ MPa ; $\beta = 0.12$; $k_p = 0.55$

τ_0 = specific molecular resistance to material dissociation

β = piezo coefficient characteristic of the molecular component of friction

k_p = constant of the microgeometry (the shape of the roughness)

The friction force will be:

$$F_f = \mu F_n = 793.2 \text{ kN}$$

The mechanical work of the frictional force will be:

$$L_f = F_f \times 0.5 \text{ m} = 396.6 \text{ kJ}$$

The total reaction force in the axial direction of the device will be:

$$R = F_n(\sin\alpha + \mu\cos\alpha) = 1257.2 \text{ kN}$$

In this case, the total mechanical work will be: $L_t = L_e + L_f = 639.7$ kJ.

Moreover, it is observed that the value of the theoretical mechanical work of R on the 0.8 m is 628.6 kJ, only 1.8 % less than L_t.

Chapter 4
Realization and analysis of the virtual model of the impact energy absorbing element on railway vehicles

4.1. Realization by means of the finite element method of the analysis of a virtual model of the impact energy absorption element on railway vehicles

4.1.1. The axially symmetric virtual model of the impact energy absorption element on railway vehicles made with the help of ANSYS

Realization by means of the finite element method (FEM) of a virtual model of the impact energy absorbing element it is a necessary step in order to extrapolate it to other dimensional variants or constituent materials, without the need for another experimental validation.

In this sense, initially it was aimed to create a virtual model with the help of the ANSYS program, having the same dimensions and using the same materials as those of the prototypes tested in the laboratory, the aim being to obtain similar results to the experimental ones, but also to the analytically calculated ones, only thus being able to ensure validation of the virtual model.

Since the impact energy absorption element by controlled plastic deformation has an axial symmetry (being an assembly of bodies of rotation), the choice of a two-dimensional virtual model was preferred which, in addition to simplicity, also has the advantage of allowing a digital calculation faster, the results being theoretically identical to those obtained by using a three-dimensional virtual model.

The friction coefficient used in MEF was calculated separately for the two variants modeled in ANSYS. Thus, for the small diameter pipe, the friction coefficient used was 0.57, while for the large diameter pipe, a friction coefficient of 0.53 was used.

The coefficient of friction was estimated using the molecular-mechanical theory of sliding friction, taking into account the fact that, when the surfaces contact, the roughnesses overlap and there is no lubricating liquid. Thus, the global friction coefficient is made up of a molecular component, caused by the need to overcome the forces of molecular adhesion, and a mechanical component, produced by the realization of the forces of plastic deformation of the roughness.

The geometry of the bodies was created two-dimensionally in Design Modeler in ANSYS, both in the case of the elements used in the experimental tests and in that of the designed and analytically calculated elements.

The initial geometric model had all the sharp edges of the bodies, and upon the contact of the pipe with the penetrator, a large plastic deformation

appeared, with material breaking, thus generating a singularity in the solution of the system of equations within the MEF, which is no longer convergent.

Therefore, the geometry was refined so that the sharp edges of the contact surfaces are connected with a radius of 5 mm to the pipe and a radius of 10 mm to the penetrator, in this case there are no more convergence problems of the solution.

Contact detection was set for a body-to-body distance of less than 0.01 mm edge-to-edge. The handling of the interface between bodies has been adjusted for touching between them. The formalization of the interaction was described by a system of extended Lagrange equations.

Figures 43 and 44 show the sketches of the body assemblies used both in the experimental tests and in the analytical calculation (the penetrator variant with a tip angle of 40^0).

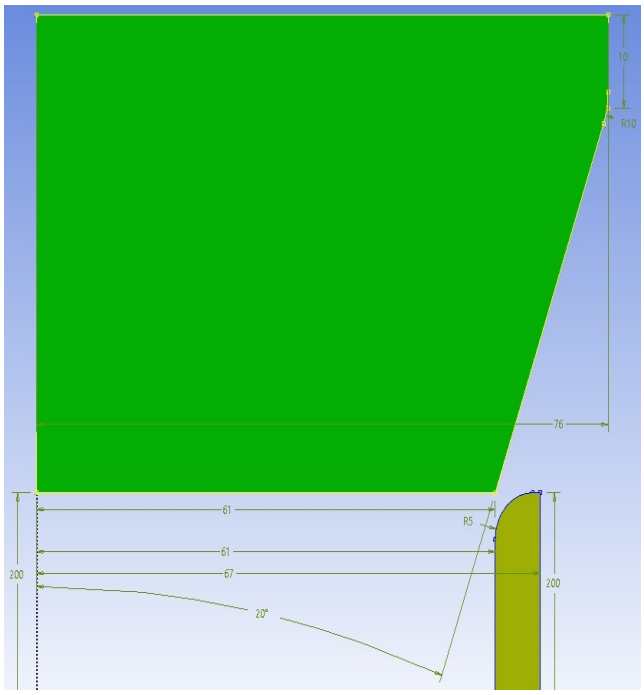

Fig. 43 *- Geometry of the assembly of bodies penetrator + small round pipe*

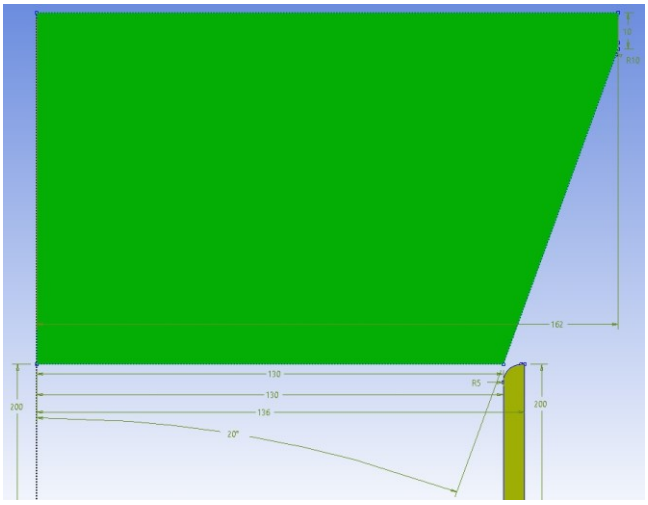

Fig. 44 *- Penetrator body assembly geometry + large round pipe*

The frictional contact surfaces (2D edges) are shown in figure 45.

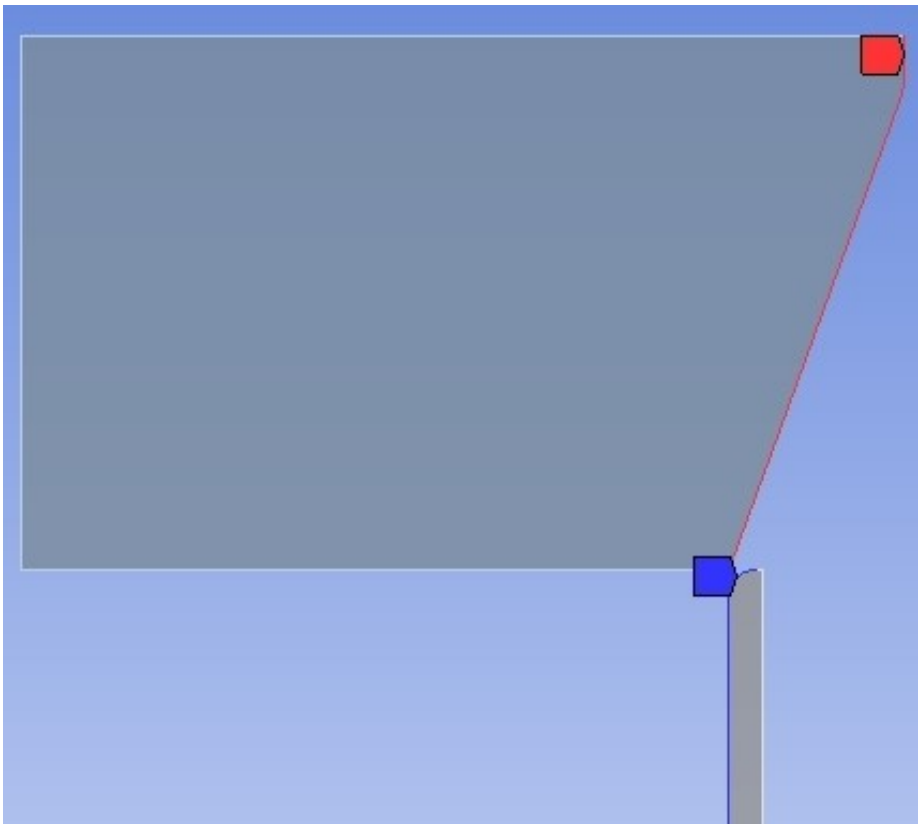

***Fig. 45** - Body assembly contact*

The properties of the material from which the penetrator was made are shown in table 6.

***Table 6** - Penetrator material properties*

Properties of Outline Row 3: Structural Steel

	A	B	C	D	E
1	Property	Value	Unit		
2	Material Field Variables	Table			
3	Density	7850	kg m^-3		
4	⊞ Isotropic Secant Coefficient of Thermal Expansion				
6	⊟ Isotropic Elasticity				
7	Derive from	Young's Modulus and Poisson's Ratio			
8	Young's Modulus	1,9E+11	Pa		
9	Poisson's Ratio	0,28			
10	Bulk Modulus	1,4394E+11	Pa		
11	Shear Modulus	7,4219E+10	Pa		
12	⊞ Strain-Life Parameters				
20	⊞ S-N Curve	Tabular			
24	Tensile Yield Strength	540	MPa		
25	Compressive Yield Strength	540	MPa		
26	Tensile Ultimate Strength	780	MPa		
27	Compressive Ultimate Strength	0	MPa		

The properties of the material from which the pipe was made are presented in table 7.

Table 7 *- Pipe material properties*

Properties of Outline Row 4: teava

	A	B	C	D	E
1	Property	Value	Unit		
2	Material Field Variables	Table			
3	Density	7850	kg m^-3		
4	Isotropic Elasticity				
5	Derive from	Young's Modulus and Poisson's Ratio			
6	Young's Modulus	2,1E+11	Pa		
7	Poisson's Ratio	0,28			
8	Bulk Modulus	1,5909E+11	Pa		
9	Shear Modulus	8,2031E+10	Pa		
10	Bilinear Isotropic Hardening				
11	Yield Strength	2,35E+08	Pa		
12	Tangent Modulus	1,05E+09	Pa		
13	Tensile Ultimate Strength	3,6E+08	Pa		

The theoretical variation curve of the normal stress **σ** in the material, depending on the specific linear strain **ε**, beyond the conventional yield threshold, is presented in figure 46.

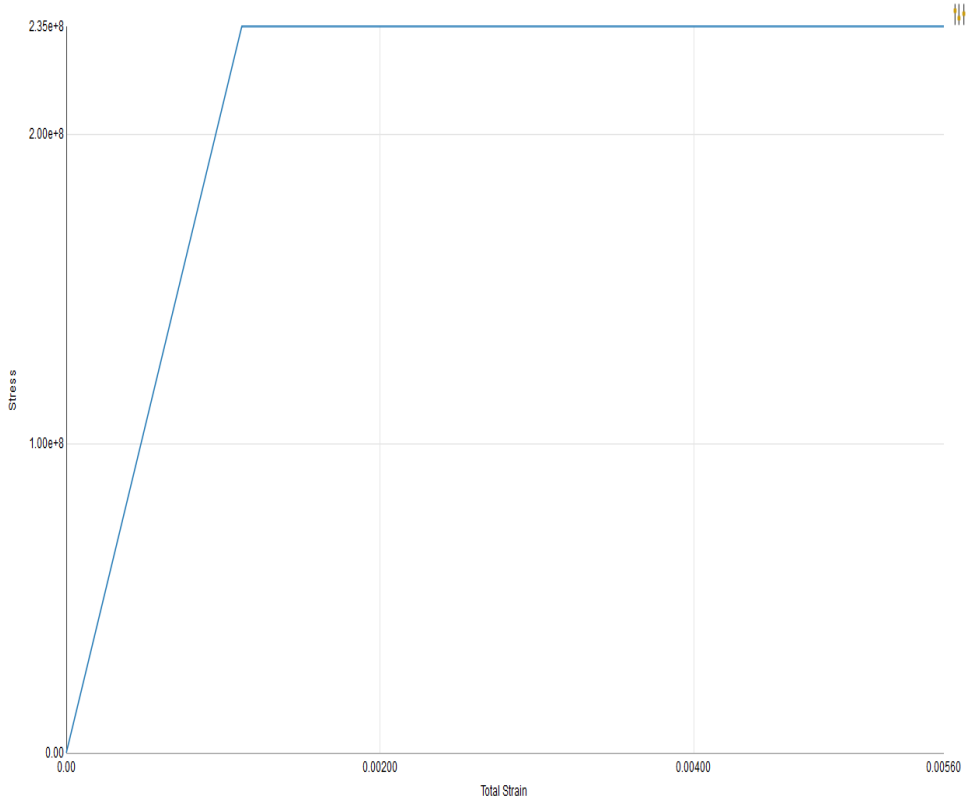

Fig. 46 *- Bilinear theoretical characteristic curve of the material*

The choice of this type of model is close to the assumption used in the analytical calculation, where controlled type plastic deformation occurs on the landing beyond the conventional yield point of the material.

The value chosen for the slope of this line is $E_p = E / 200$. This value was not chosen randomly, but based on Annex C (analysis by the finite element method) of the standard "SR EN 1993-1-5:2007+AC:2009", regarding the design of steel structures, as well as based on experimental studies on the behavior of structural steels beyond the yield point.

Figure 47 shows an experimental model of the stress-strain curve for a structural carbon steel.

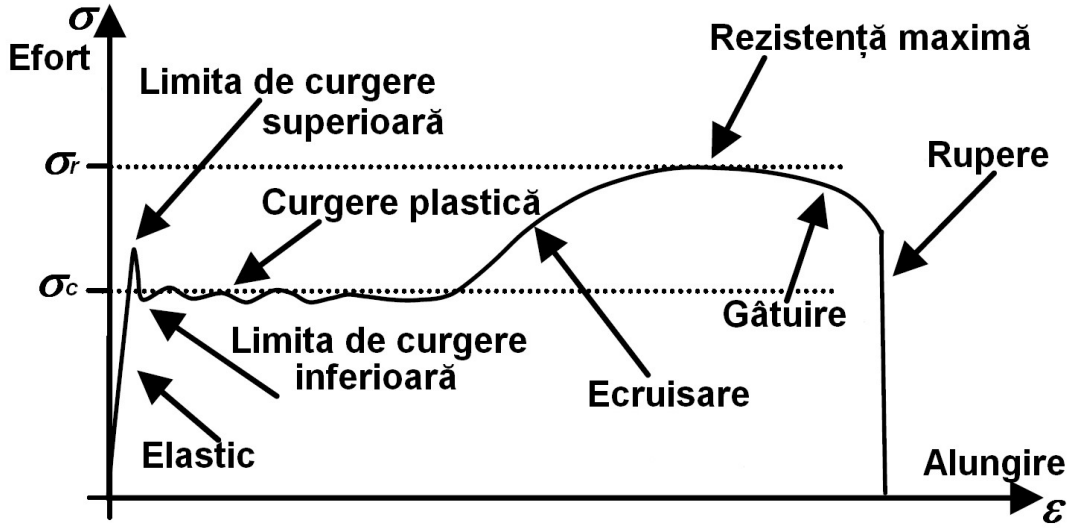

***Fig. 47** - Experimental normal stress variation curve depending on the specific elongation*

The experimental curve above can be theoretically approximated with the one shown in figure 48.

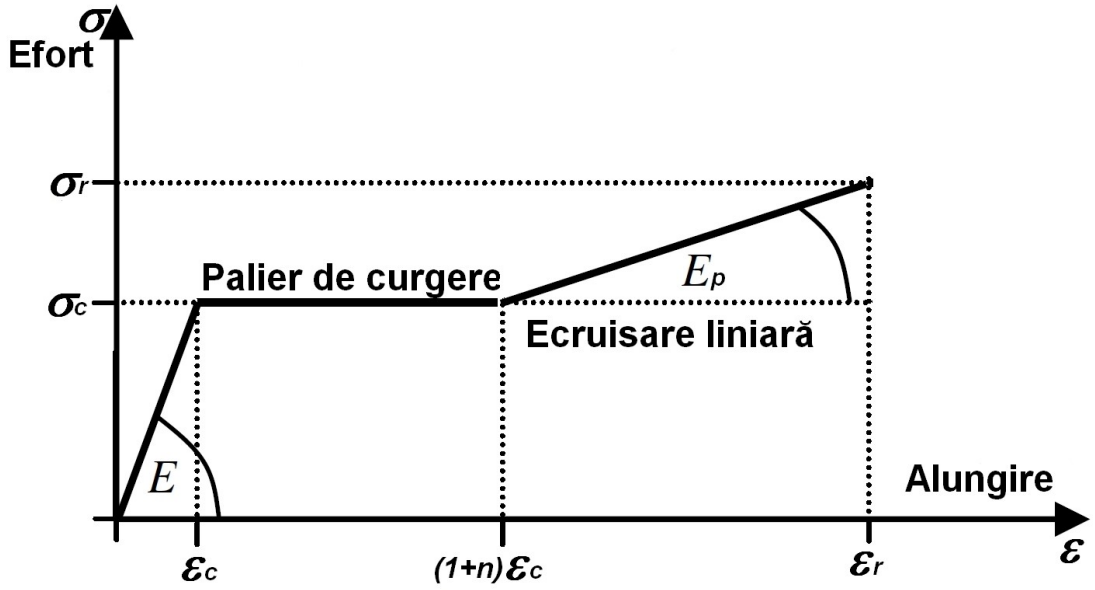

***Fig. 48 -** Theoretical normal stress variation curve depending on the specific elongation*

If n = 0, we no longer have a flow level and the theoretical curve is reduced to a bilinear one. In this case we have the following calculation relations:

$E = \sigma_c / \varepsilon_c$ and $E_p = (\sigma_r - \sigma_c) / (\varepsilon_r - \varepsilon_c)$, and $h = E_p / E = 0.5$ %;

where $h = (\sigma_r/\sigma_c - 1) / (\varepsilon_r/\varepsilon_c - 1)$, was calculated based on experimental determinations for S235JR type carbon steel.

Following the extensive analysis carried out with MEF, for h = 1 % it was found that the reaction force increased more than 1.5 times, compared to the one measured experimentally, while for h = 0.1 %, the reaction force decreased by almost 40 % compared to the experimentally measured one.

Figures 49 and 50 show the difference between the pipe deformation when a bilinear isotropic behavior was chosen in the flow area (which respects the experimental deformation allure), compared to a bilinear kinematic one.

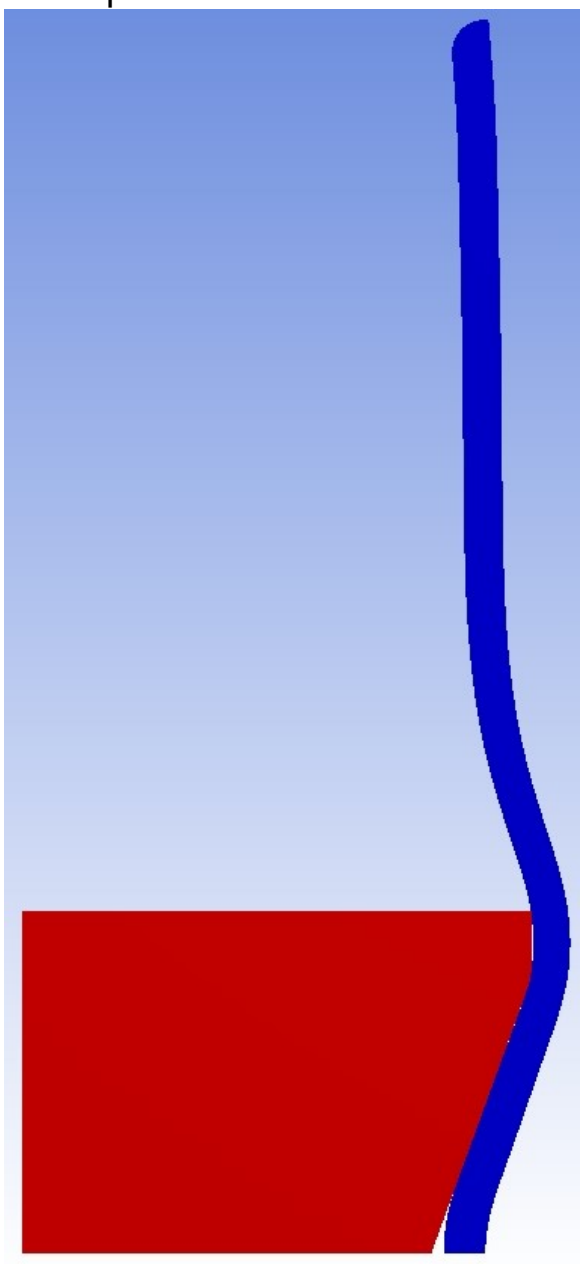

Fig. 49 - *Kinematic deformation*

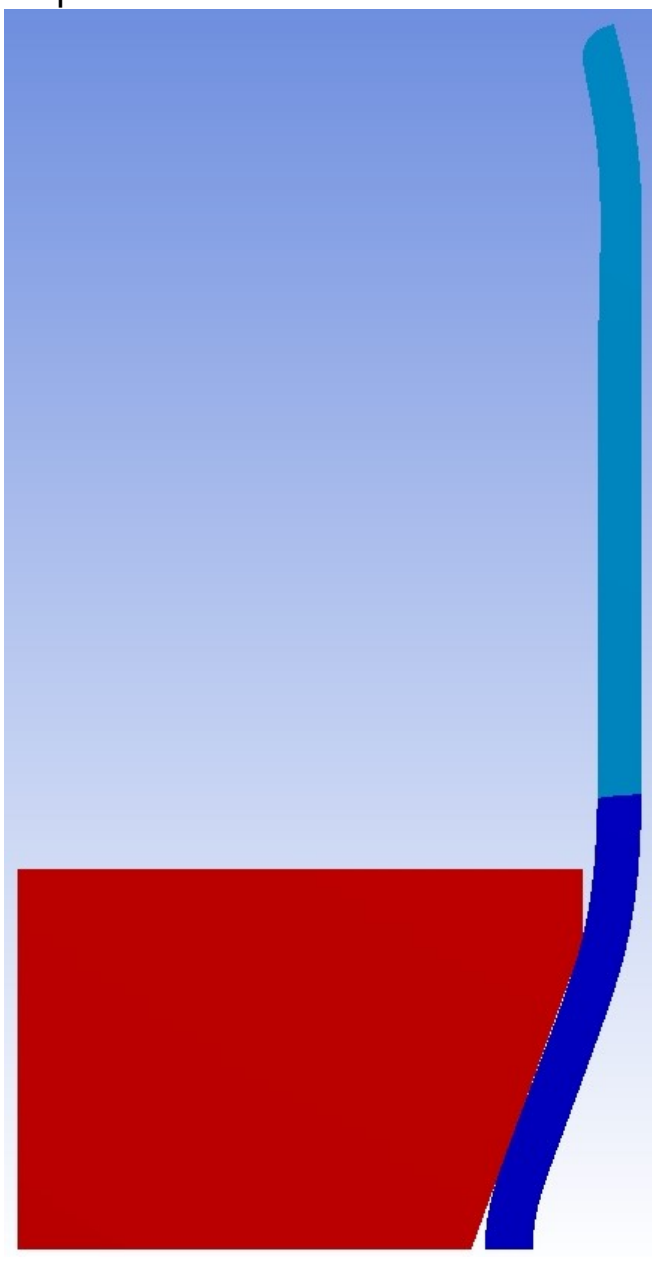

Fig.50 - *Isotropic deformation*

4.1.2. Discretization of the model of the impact energy absorption element on railway vehicles

The model of the assembly of the two bodies (cylindrical pipe and tapered penetrator), which make up the impact energy absorption element, was discretized mostly with quadrilateral elements, but also with some triangular elements:

- The discretization started from 10 mm size elements, the penetrator having relatively large dimensions and extremely small deformations compared to the pipe;
- Optimization of the solution time of the available computing system was also pursued - Intel Pentium DualCore G4400 at the frequency of 3.3 GHz and 8 GB RAM, with Windows 10 Pro 64-bit operating system;
- The edges in the contact area between the penetrator and the pipe benefited from a finer specific discretization (figure 51), the size of the elements being automatically adapted by the program, to achieve an optimal discretization quality. Thus, the largest elements in the pipe had a size of about 1 mm;
- Transitions were slow and with a high degree of smoothness;
- Non-linear calculation with large displacements was preferred;
- Curvature and edge proximity detection has been enabled.

In the discretization version of the model using the automatic method, it was imposed that the starting size of the elements be 2.7 mm in the case of the small diameter pipe, respectively 4.2 mm in the case of the large diameter pipe, so as to obtain a number as close as possible to nodes and elements, comparable to the previous case (fig. 52).

Table 8 shows the values determined by MEF for the two discretization modes and for the two pipe sizes.

Table 8 *- Values determined by MEF for two discretization modes*

d [mm]	Discretization	R [kN]	Nodes	Elements	Observations
122	Edges	596,5	2723	791	R analytic = 564,6 kN
	Automated	580,8	2706	804	R experiment = 591,5 kN
262	Edges	1237,8	3667	1093	R analytic = 1257,2 kN
	Automated	1225,5	14783	4497	

From the above, it is noted that the values of the reaction force, obtained in the case of the specific discretization of the contact edges, are closer to the analytically calculated or experimentally determined reaction force values, than those obtained in the case of the automatic discretization.

In conclusion, for approximately the same number of nodes and elements, the results obtained have a higher accuracy in the case of using a specific discretization adapted to the geometry of the bodies, than in that of an automatically generated one.

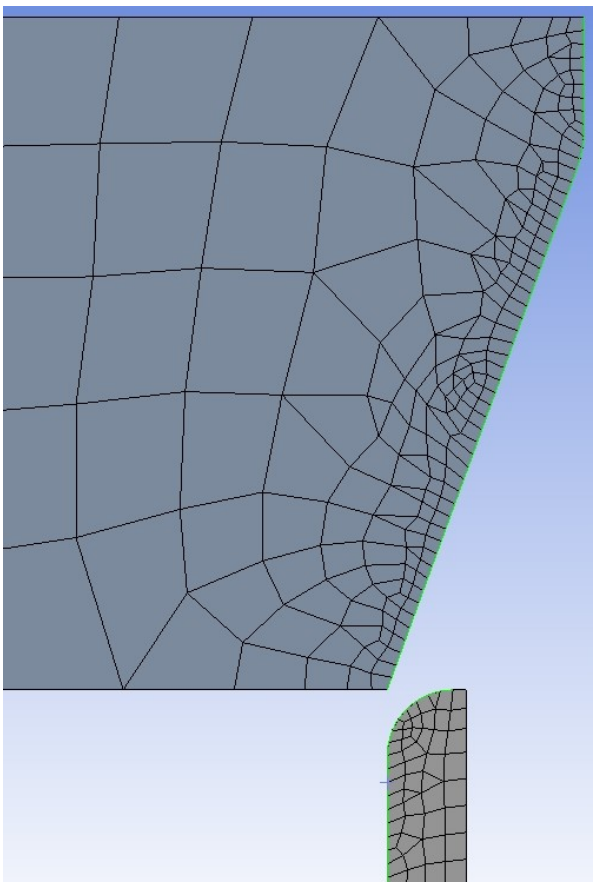

Fig. 51 - *Detail of discretization of contact edges*

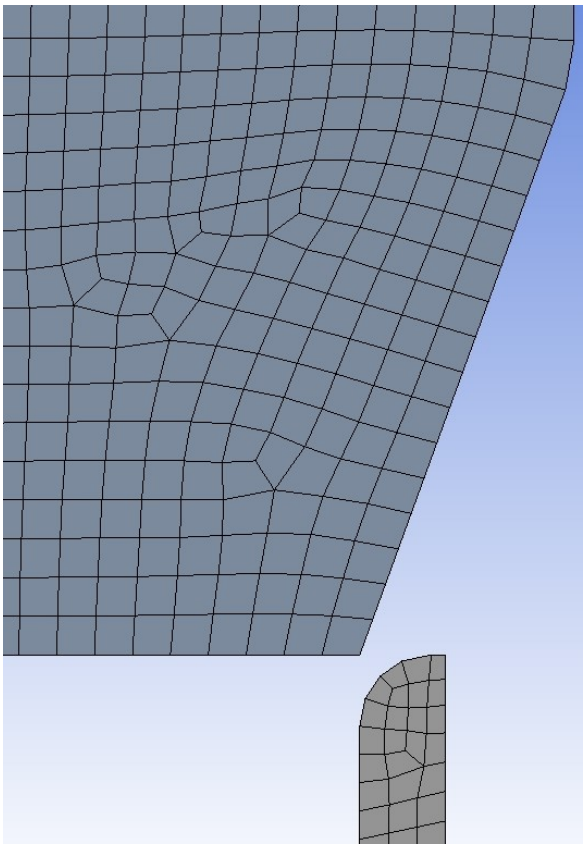

Fig. 52 - *Detail of automatically generated discretization*

4.2. Analysis of the plastic mechanical deformation when the impact energy absorption element flares out on railway vehicles

4.2.1. Establishing the constraints limiting the movement of bodies and the parameters of the analysis by the finite element method

For the study of the plastic mechanical deformation of the impact energy absorption element, a static structural analysis was used using the ANSYS Workbench module.

First of all, a series of constraints was established regarding the limitation of the movement of the assembly of bodies. Thus, it was imposed to block the movement of the lower surface of the pipe in the vertical direction, because it is supported in reality on a fixed base plate, constituted by the front cross-beam of the wagon chassis.

It was also imposed to limit the movement of the penetrator only in the vertical direction and only along the length of the pipe, until it reaches the front cross-beam of the wagon chassis (it cannot go down beyond the lower part of the pipe).

An analysis with a direct type solution was chosen, in which large deformations should be taken into account. The chosen numerical solution method was non-symmetrical Newton- Raphson (tangent method for quadratic convergence). Both force and displacement convergence have been enabled.

The imposed vertical displacement was performed in one step for which the final time was fixed at t_f = 50 s (in accordance with the duration of the experimental test).

4.2.2. The results obtained from the MEF analysis

The deformation of the pipe at t = 25 s is shown in figure 53.

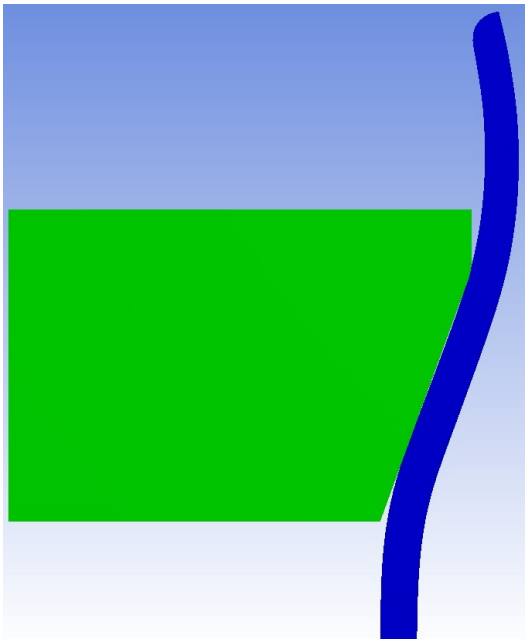

Fig. 53 - *Detail of the pipe deformation at t = 25 s*

It is observed that in the lower part of the penetrator, the contact with the pipe occurs higher than the small base of the truncated cone, while, on the upper cylindrical segment, the contact is lost due to the bending of the pipe walls. The general shape of the pipe deformation is similar to that obtained experimentally.

The synthesis of the results obtained for the main monitored parameters can be found in table 9, where the results obtained through the analytical calculation of the theoretical model, through experimental determinations and through the two variants of the MEF analysis are compared.

Table 9 *- Comparison of obtained results*

Models	α	μ	d [mm]	R_m[kN]	Observații
Analytical	40^0	0,57	122	564,6	Diferă cu 4,8 % de R_{exp} = 591,5 kN
		0,53	262	1257,2	Valoare de referință țeavă mare
MEF analysis		0,57	122	596,5	Diferă cu 0,8 % de R_{exp} = 591,5 kN
		0,53	262	1237,8	Diferă cu 1,6 % de R analitic
Experi-mental	40^0	-	122	591,5	Valoare de referință țeavă mică
	50^0	-		-	Materialul a cedat prematur, țeava pierzându-și stabilitatea.
	60^0	-		-	

Since, for the angles of 50^0 and 60^0, no relevant experimental results were obtained, the analysis of these cases through MEF was abandoned, the results thus obtained could not be useful in the absence of comparison values.

The value of the resultant force in the vertical direction was averaged from both experimental and MEF results.

The criterion used was that it be quasi-constant on a plateau with a duration of about 17 s, the difference between two consecutive values being less than 0.2 %. This time interval was chosen according to the duration of the experimentally determined plateau. In this way, a number of 68 values obtained through MEF were averaged, four per second.

Figure 54 shows the time variation curve of the resultant vertical force, obtained experimentally for the penetrator with a tip angle of 40^0.

By carefully analyzing this curve, compared to those in figures 55 and 56 (the time variation of the vertical resultant force obtained by MEF for both pipe sizes), it is found that all the variation curves are similar, which indicates a similar behavior, correctly described by MEF.

Thus, after approximately the first two seconds, a first inflection is observed in the rapid quasi-linear increase in force (about 150 kN/s), which denotes the transition from an elastic behavior of the pipe walls (with the advance of the penetrator) to a plastic one. The force increase continues at a somewhat slower ramp of about 30 kN/s until the penetrator is fully inserted into the pipe, at which point the force reaches a quasi-horizontal plateau.

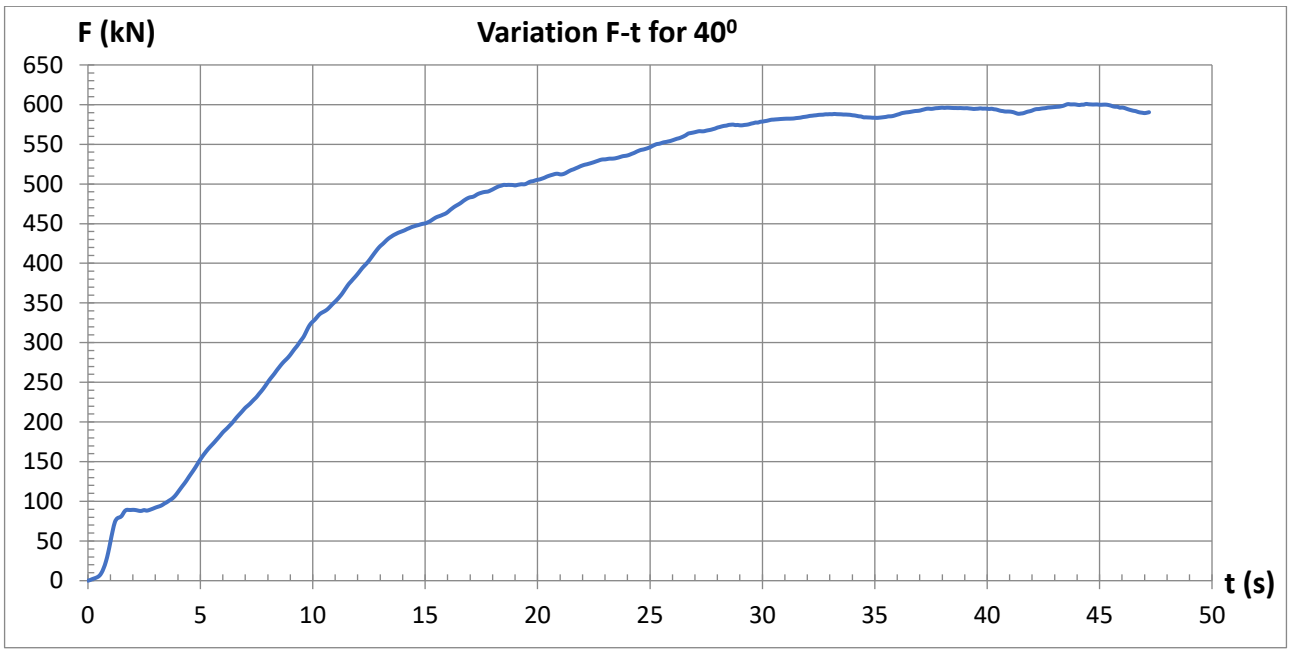

Fig. 54 - *The vertical force-time variation curve, obtained experimentally*

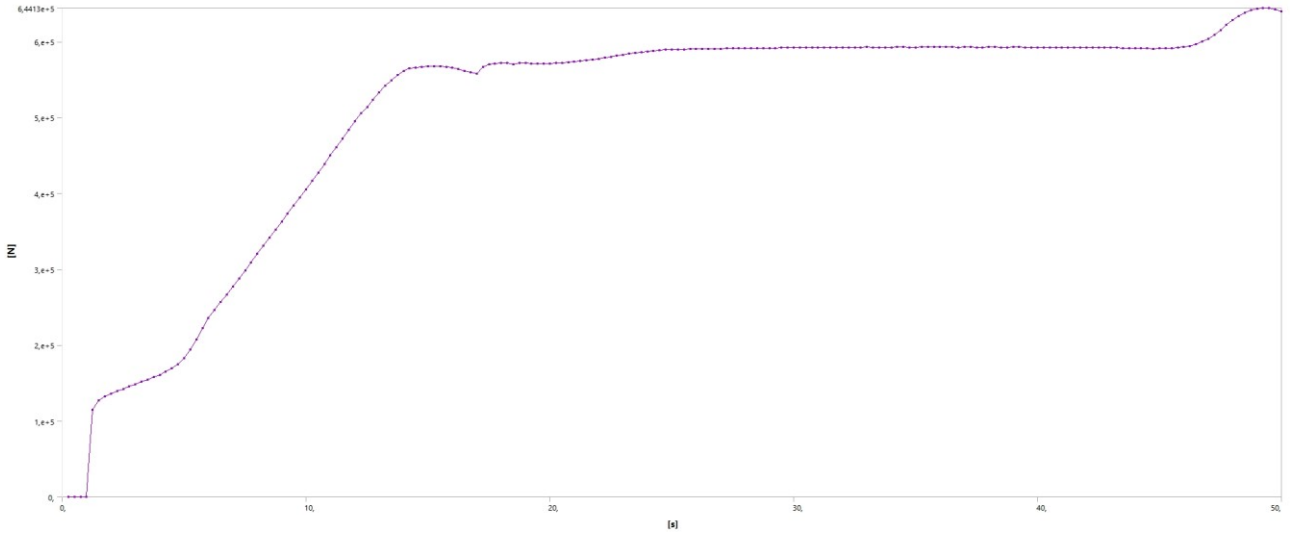

Fig. 55 - *Time variation curve of the resultant vertical force obtained for the small diameter pipe*

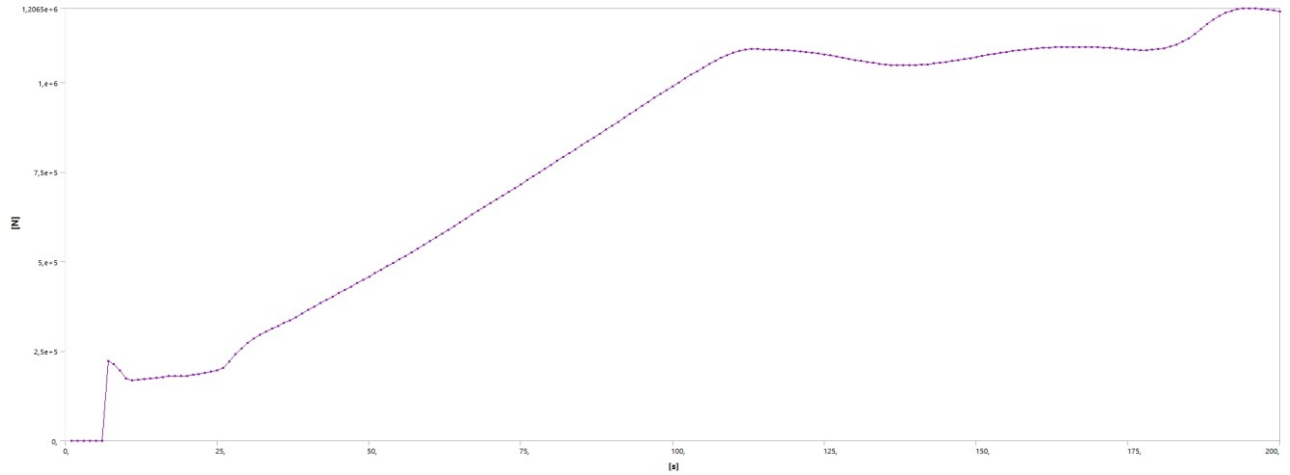

Fig. 56 - *Time variation curve of the resultant vertical force obtained for the large diameter pipe*

Chapter 6
General conclusions

5.1. Final conclusions

The collision of two railway vehicles can be classified as inelastic central binary collisions (type I - with energy absorption), in which the final kinetic energy of the bodies is lower than the initial one.

The reaction energy Q is considered to be dissipated during the collision only through the mechanism of controlled plastic deformation, the other forms of energy dissipation (thermal, elastic oscillatory damped by the vehicle suspension) being much lower and can be neglected.

The considered decelerations did not exceed 5 g, thus avoiding the possible occurrence of human casualties caused by the shock received following the collision, and the forces that occurred during the collision were below the plastic deformation limit of the resistance structure of the railway vehicle.

In order to satisfy the need to absorb through plastic deformation a large amount of energy resulting from the impact, the material chosen was an unalloyed steel with good plasticity (high tensile elongation and low yield strength) and increased toughness (high resilience, i.e. high energy absorbed during shock bending).

The optimal shape chosen for the energy-absorbing element was the cylindrical one, because it absorbs more energy in the case of plastic deformation and because it better resists buckling, showing symmetry around the longitudinal axis, but also against all diametrical planes perpendicular to the bases, and thus providing a good and equal resistance.

Following the calculations, it was noted that the energies dissipated for bending and chipping are relatively comparable, but much lower than those for expansion and friction, which are strongly influenced by the change of the angle of the penetrator, the thickness of the pipe wall or the condition of the contact surfaces (degree of lubrication or roughness).

The researches carried out proved that the advanced proposal for the realization of some structural elements dedicated to the absorption of impact energy in railway vehicles is feasible from a technical point of view, both the analytical calculations and the virtual model developed through MEF, being validated by the results obtained experimentally on a model at reduced scale. The proposed solution can cover the absorption of impact energy in more than 75 % of frontal collision cases, for speeds up to 15 m/s, for all types of railway vehicles, and in the case of passenger cars, it can cover them completely.

5.2. Personal contributions

In order to achieve the goals proposed in this work, it was necessary to complete some research internships with a high degree of complexity, thus the work brings a number of personal contributions, among which I mention:

- the provision of an innovative constructive variant, which ensures the increase in the impact energy absorption capacity of railway vehicles;

- to satisfy the need to absorb through plastic deformation a large amount of energy resulting from the impact, the material chosen was an unalloyed steel, with good plasticity (high tensile elongation and low yield strength) and increased toughness (high resilience - high energy absorbed during shock bending);

- in the buffering experiment of two freight wagons, having almost identical masses, one of which was stationary, a test carried out at the Făurei Railway Testing Center of the Romanian Railway Authority, to calculate the speed of the moving wagon, immediately before the collision, was measured, with a specially adapted timer, the duration of the successive passage of the axles of the same bogie through the same landmark, fixed on the sole of the rail and equipped with a microswitch triggered when the lip of the wheelband passes over it;

- the same speed was determined by video analysis of the crash test recording, at the filming speed of 30 frames/second, with a camera fixed on a tripod, by determining the movement of the wagon between two successive frames, taking into account a fixed landmark. The two values obtained were similar, which allowed the use of the second method in determining the speed of the assembly of the two wagons immediately after the collision;

- following the plastic deformation test of a pipe by expansion, test carried out at the Innova company Systems & Technologies from Arad, it was observed that the value of the mechanical work, obtained experimentally, for the plastic deformation of the pipe, is similar to the one obtained by the analytical calculation, and the value of the average compression force differs by less than 5 % from the analytically calculated value;

- carrying out the numerical analysis of the new structural solutions and studying the behavior of these structures, by determining the state of tension and deformation generated by the application of some loads provided in the reference documents in force.

The advantage of developing the virtual model lies mainly in the ease of its extrapolation to the real scale, as well as in the parameterization of the main defining technical characteristics (dimensions, materials, boundary conditions for borders and contacts, etc.), in order to adapt as easily as possible to the various requirements of manufacturers, eliminating the need for numerous expensive experimental tests until the series 0 prototype is validated.

The reading of the two-dimensional virtual model was possible due to the fact that the element of impact energy absorption by plastic deformation of controlled type has an axial symmetry (being an assembly of bodies of rotation).

This model, in addition to its simplicity, also has the advantage of allowing a faster calculation than by using a three-dimensional virtual model.

The geometric model has been refined so that the sharp edges of the contact surfaces are connected to both the pipe and the penetrator, in this case there are no more solution convergence problems caused by the appearance of a singularity in solving the system of equations within the MEF, generated

by the abrupt contact between the bodies.

For the flow zone of plastically deformed material, the choice of a bilinear isotropic behavior in the model versus a bilinear kinematic one led to the observance of the experimental deformation allure.

Also, the refinement of the discretization at the edges of the contact zone of the bodies and the use of the smallest possible size of the finite elements led to the optimization of the model discretization.

All this led to a higher accuracy of the obtained results, in the sense that the reaction force values calculated by the program were very close to the analytically calculated or experimentally determined reaction force values.

Therefore, the theoretical calculation model adopted is validated by the results obtained experimentally, which allows its extrapolation also in the case of using pipes with different dimensions, in order to obtain a maximum absorption of the impact energy, by transforming it into mechanical work of plastic deformation controlled type.

At the same time, the model made by MEF is validated both by the results obtained experimentally and by those obtained by analytical calculation, which allows very easily its parameterization to establish the behavior of a wide variety of impact energy absorbing elements.

In this paper have been proposed solutions with a high degree of applicability in the field of transport, regarding the increase of the impact energy absorption capacity of railway vehicles, rigorously argued solutions from a scientific point of view, numerically and experimentally, their application being able to lead to the improvement of railway transport safety and to benefits for the socio-economic environment.

5.3. Future research directions

The theme proposed by this paper is particularly promising for the future development of new research directions, of which a few major ones can be listed:

- improving and refining the model developed by MEF with the aim of bringing the obtained simulation as close as possible to reality;
- testing several prototypes, having different gauges (diameters and wall thicknesses), in order to have several comparative results;
- testing several penetrators with different tip angles;
- testing several types of materials, both ferrous and non-ferrous, but also several shapes of profiles, to maximize the absorption of impact energy through their plastic deformation in a controlled manner;
- development of a model by MEF for the controlled absorption of impact energy by chipping;
- development of a model by MEF for the controlled absorption of impact energy by bending;
- testing several prototypes, with different numbers of cutting knives and implicitly bending zones;
- combining several methods of impact energy absorption through controlled plastic deformation.